



Universidade do Minho
Escola de Engenharia

Muhammad Hussam Khaliq Key Features of Materials for the Fused Deposition Modelling Process

Muhammad Hussam Khaliq

Key Features of Materials for the
Fused Deposition Modelling Process

UMinho | 2015



junho de 2015



Universidade do Minho
Escola de Engenharia

Muhammad Hussam Khaliq

Key Features of Materials for the
Fused Deposition Modelling Process

Dissertação de Mestrado
European Masters in Engineering Rheology

Trabalho efetuado sob a orientação do
Professora Doutora Olga Sousa Carneiro
Professor Doutor Luis Lima Ferrás



junho de 2015

DECLARAÇÃO

Nome: Muhammad Hussam Khaliq

Correio electrónico: hussamkhaliqs@gmail.com

Número do Passaporte: LB4125701

Título da dissertação:

Key Features of Materials for the Fused Deposition Modelling Process

Ano de conclusão: 2015

Orientador(es): Prof. Olga Sousa Carneiro and Dr. Luis Lima Ferrás

Designação do Mestrado:

European Masters in Engineering Rheology

É AUTORIZADA A REPRODUÇÃO INTEGRAL DESTA DISSERTAÇÃO APENAS PARA EFEITOS DE INVESTIGAÇÃO, MEDIANTE DECLARAÇÃO ESCRITA DO INTERESSADO, QUE A TAL SE COMPROMETE.

Guimarães, ___ / ___ / _____

Assinatura: _____

Acknowledgments

All praise to **God Almighty**, who provided me the necessary strength to accomplish this project. All respects are for the creator of this universe, whose teachings are true source of knowledge & guidance for whole mankind.

Before anybody else I thank my **Parents** who have always been a source of moral support, driving force behind whatever I do. I am indebted to my project advisors **Prof. Olga Sousa Carneiro** and **Dr. Luis Lima Ferrás** for their encouragements, technical discussions, inspiring guidance, remarkable suggestions, keen interest, constructive criticism and friendly discussions which enabled me to complete this project. I would also like to thanks **Prof. Miguel Nobrega** for his kind suggestions throughout the project. They also spared a lot of precious time in advising & helping me in writing this report.

I am also thankful to the technicians (Eng. Maurício and João Paulo) and researchers (Eng. Rui Gomes, Dr. Sacha Mould and Eng. Paulo Teixeira) of the Polymer Engineering Department, University of Minho, for their cooperation and help during different tests.

Author

Abstract

In this work, different acrylonitrile butadiene styrene (ABS) samples (grades) are studied in order to check if the ABS used in the fused deposition modelling process has some special characteristics, or, any ABS material can be used instead. The different samples of ABS used in this study include a commercial ABS in the form of pellets used for conventional polymer processing and three ABS samples in the form of filaments that are used in different fused deposition modelling processes.

The rheological characterization of these materials is done using a stress controlled rotational rheometer (Paar Physica MCR 300) and a twin bore capillary rheometer (Rosand RH10). From the rheological characterization one could find that the pelleted ABS sample is much more viscous and elastic than the other three samples of ABS. Therefore, only two different ABS samples were used for 3D printing of pre-defined geometry specimens using the fused deposition modelling process (the pelleted ABS and one of the ABS samples in the form of filament). These 3D printed specimens were mechanically and optically analysed using the universal testing machine, INSTRON 4505, the stereoscopic magnifying glass Olympus and the digital camera Leica. This way the sintering and adhesion achieved between the extruded filaments of feedstock material for the different samples could be evaluated, and, the results obtained revealed to be in accordance with the statements made based on the rheological results.

Lastly, the numerical modelling of the flow of the polymer melt in the nozzle (liquefier) of the fused deposition modelling machine was performed, in order to check the differences between the two different materials behaviour.

It was concluded that the ABS used in fused deposition modelling process needs to have pre-defined controlled rheology.

Resumo

Neste trabalho, diferentes tipos de amostras de acrilonitrilo-butadieno-estireno (em inglês *acrylonitrile butadiene styrene* (ABS)) são estudados com o intuito de verificar se o ABS usado no processo de FDM (em inglês *Fused Deposition Modelling*), tem ou não características especiais, ou, qualquer tipo de ABS pode ser usado neste processo de impressão. As diferentes amostras de ABS usadas neste estudo são: o ABS comercial na fórmula de grânulos, que normalmente é usado nos processos convencionais de processamento, e, três amostras de ABS na forma de filamentos, que, são usados em diferentes processos de FDM.

A caracterização reológica destes materiais é feita usando um reómetro rotacional de tensão controlada (Paar Physica MCR 300) e ainda um reómetro capilar (Rosand RH10).

Dos resultados obtidos através da caracterização reológica foi possível concluir que o ABS na fórmula de grânulos é muito mais viscoso e elástico que as outras três amostras de ABS. Então, por forma a evitar o tratamento demasiado extensivo dos resultados, apenas duas amostras foram impressas na impressora 3D usando o método de FDM (para a impressão de objectos com geometria predefinida). As amostras escolhidas foram então o ABS na fórmula de grânulos e uma das amostras de ABS na forma de filamento.

As geometrias impressas foram submetidas a testes mecânicos e ópticos usando a máquina INSTRON 4505, usando a lupa estereoscópica da Olympus e a câmara digital Leica. Desta forma, foi possível avaliar a qualidade de sinterização e adesão entre os filamentos extrudidos, para as diferentes amostras. Os resultados obtidos revelaram estar de acordo com as conclusões tiradas através dos resultados reológicos.

Neste trabalho foi ainda feito um estudo de modelação numérica do polímero “fundido” no interior da impressora, permitindo assim fazer uma análise detalhada do escoamento nesta geometria, para as duas amostras estudadas.

Como conclusão final, podemos dizer que o ABS usado no processo de FDM necessita de uma reologia pré-definida.

Table of Contents

Acknowledgments.....	iii
Abstract.....	v
Resumo.....	vii
List of Figures	xi
List of Tables.....	xiv
Part I Bibliographic Review	1
1. Introduction.....	2
1.1. Fused Deposition Modelling.....	5
1.2. Motivation/ Objectives.....	8
1.3. Route to Objectives	8
1.4. Thesis Structure	9
2. Materials and Methods	10
2.1. Materials.....	10
2.2. Basic Concepts: Rheology and Rheometry.....	13
2.3. Thermal Characterization/Analysis	17
2.4. Production of Specimens.....	20
2.4.1. Extrusion of Filament	20
2.4.2. 3D Printing Process	21
2.5. Characterization of Specimens.....	23
3. Basic concepts: Equations and Modelling.....	24
3.1. Newtonian and Generalized Newtonian Fluids.....	24
3.2. Viscoelastic Fluids.....	25
Part II Experiments, Results and Discussion	29
4. Experimental Results and Discussion	30
4.1. Rheological Testing.....	30
4.1.1. Sample 1.....	31
4.1.2. Sample 2.....	32
4.1.3. Sample 3.....	34
4.1.4. Sample 4.....	35
4.1.5. Comparison of Different Samples	36
4.2. 3D Printing of Specimens	38

4.2.1.	Dimensions of the Specimens and Printing Pattern	38
4.2.2.	Printing Conditions.....	39
4.3.	Samples Performance.....	42
4.3.1.	Flexural Testing	42
4.3.2.	Optical Analysis	45
4.4.	Global Discussion.....	47
Part III Modelling.....		49
5.	Numerical Modelling	50
5.1.	Geometry, Simulation and Numerical Results	51
5.1.1.	Viscous Results	52
5.1.2.	Viscoelastic Results	54
Part IV Conclusions.....		57
Conclusions and Future Work.....		58
Bibliography		61

List of Figures

Figure 1 : Fused Deposition Modelling process, adapted from (CustomPartNet 2009)	3
Figure 2 : Stereo Lithography with its components, adapted from (Proto3000 2013)	4
Figure 3 : Selective Laser Sintering and its different parts, adapted from (Treehugger 2015)	5
Figure 4 : Linear Polymer with Entanglements, adapted from (W.J. Briels 1998).....	10
Figure 5 : Cross-linked Polymer, adapted from (Donna Narsavage-Heald n.d.).....	11
Figure 6 : Different types of Polymers, where, a small bead represents the monomer unit. Adapted from (Adhesivesandglues.com 2012)	11
Figure 7 : Amorphous and Crystalline structures, where small beads represent the monomer units. Adapted from (Adhesivesandglues.com 2012).....	11
Figure 8 : Different structures of copolymers, where A and B are the different monomer units, adapted from (Fried 2014).....	12
Figure 9 : Structural formula of ABS. Adapted from (Chemical Book 2010).....	13
Figure 10 : Strain controlled rheometer. Adapted from (Jeffrey Gotro 2014)	14
Figure 11 : Stress controlled rheometer. Adapted from (Jeffrey Gotro 2014).....	14
Figure 12 : Rotational rheometers (A) Parallel plate (B) Cone and plate (C) Concentric cylinder and (D) Torsion rectangular. Adapted from (John R. Schrei 2002)	15
Figure 13 : Capillary rheometer and its basic parts. Adapted from (ASI adhesives & sealants 2003)	15
Figure 14 : Glass transition temperature of an amorphous polymer. Adapted from (Gonzalez-Gutierrez 2015)	18
Figure 15 : Melting transition of crystalline polymers. Adapted from (Gonzalez-Gutierrez 2015)	18
Figure 16 : Differential scanning calorimetry, sample pan and reference pan.	19
Figure 17 : Two DSC systems (a) Heat flux DSC, (b) Power–compensation DSC, adapted from (Bhadeshia 2002)	19

Figure 18 : Extrusion line including auxiliary equipment's (cooling system, puller and cutting system), adapted from (rediff blogs 2012) 20

Figure 19 : FDM process and its components; (1) Feed pinch rollers, (2) Liquefier/print head and (3) Build surface..... 21

Figure 20 : Flexural testing, three point bending test. Adapted from (MatWeb 2014) 23

Figure 21 : Representation of the viscoelastic behaviour with a spring and dashpot..... 26

Figure 22 : Representation of the viscoelastic behaviour with springs and dashpots (different combinations) 27

Figure 23 : Used rheometers (a) Paar physica (MCR 300), (b) Capillary rheometer Rosand (RH10)..... 31

Figure 24 : Sample 1, Low & High shear rate sweep, (low shear rate sweep performed with MCR 300, and high shear rate sweep is performed using RH10).... 31

Figure 25 : Sample 1, G' and G'' master curves at 230 °C, SAOS frequency sweep .. 32

Figure 26 : Sample 2, Low & High shear rate sweep, (low shear rate sweep performed with MCR 300, and high shear rate sweep is performed using RH10).... 33

Figure 27 : Sample 2, G' and G'' master curves at 230 °C, SAOS frequency sweep... 33

Figure 28 : Sample 3, Low & High shear rate sweep, (low shear rate sweep performed with MCR 300, and high shear rate sweep is performed using RH10).... 34

Figure 29 : Sample 3, G' and G'' master curves at 230 °C, SAOS frequency sweep... 35

Figure 30 : Sample 4, shear rate sweep at 230 °C, obtained using MCR 300 35

Figure 31 : Sample 4, SAOS frequency sweep, obtained using MCR 300 36

Figure 32 : Viscosity (shear rate sweep) comparison, at reference temperature (230 °C) 36

Figure 33 : Elastic modulus (G') comparison, at reference temperature (230 °C).... 37

Figure 34 : 3D printed specimen, length: 76 mm, width: 11 mm, and depth: 3.5 mm 38

Figure 35 : Selected 3D-Printing pattern for specimens..... 39

Figure 36 : Differential scanning calorimeter (DSC), DSC Netzsch 40

Figure 37 Sample 1: DSC results..... 41

Figure 38 Sample 2: DSC results..... 41

Figure 39 : Universal testing machine, INSTRON 4505 42

Figure 40 : Sample 1, three point bending test (flexural testing).....	43
Figure 41 : Sample 2 (50 mm/s), three point bending test (flexural testing)	44
Figure 42 : Sample 2 (30mm/s), three point bending test (flexural testing)	44
Figure 43 : Stereoscopic magnifying glass Olympus and digital camera Leica.	45
Figure 44 : Specimens printed using sample 1.....	46
Figure 45 : Specimens printed (50 mm/s) using sample 2.....	46
Figure 46 : Specimens printed (30 mm/s) using sample 2.....	47
Figure 47 : Storage modulus, loss modulus and viscosity for 230 °C (experimental data and fit obtained with the 6-mode FENE-P model for sample 2)	50
Figure 48 : Shear viscosity fit for sample 1 (left) and sample 2 (right).	51
Figure 49 : 3D printer nozzle: screw (left), schematic of the geometry where the polymer melts flows (right).	52
Figure 50 : Velocity magnitude for samples 1 (left) and sample 2 (right), along the channel.....	52
Figure 51 : Pressure for samples 1 (left) and sample 2 (right), along the channel....	53
Figure 52 : Shear stress for samples 1 (left) and sample 2 (right), along the channel.	54
Figure 53 : Normal stress for samples 1 (left) and sample 2 (right), along the channel.....	54
Figure 54 : Velocity magnitude (left) and pressure (right) along the channel for sample 2 (Viscoelastic simulation).	55
Figure 55 : Shear (left) and normal (right) stresses along the channel for sample 2 (Viscoelastic simulation).	55

List of Tables

Table 1: Different rheological tests used to characterize the rheological behaviour of materials.....	17
Table 2 : Samples (grades) of acrylonitrile butadiene styrene (ABS) used in this study	30
Table 3 : Process parameters used in fused deposition modelling (3D printing)	39
Table 4 : Glass transition temperatures of ABS samples	40
Table 5 : Sample 1, results of three point bending test (maximum loads at breakage)	43
Table 6 : Sample 2 (50 mm/s), results of three point bending test (maximum loads at breakage)	44
Table 7 : Sample 2 (30 mm/s), results of three point bending test (maximum loads at breakage)	45
Table 8: Parameters used in the 6-mode FENE-P model fit.....	51

Part I Bibliographic Review

Chapter 1

1. Introduction

The idea of printing goes back to the early Mesopotamian civilization before 3000 BCE, where round seals were used to print on clay tablets. Since then, printing techniques have evolved and diversified, leading, for example, to the portable ink printers that we have nowadays in our homes. Although the word “printing” is strongly associated to these ink printers, this is merely a consequence of our common sense, since “printing” embraces a broad range of techniques. Basically, different printing techniques were developed based on the personal or the group needs. For example, printing in clothes, or the mass printing of books and newspapers. With the exponential growth of technological progress and the change in people’s needs, 3D printing became a reality, allowing to print cars or even houses.

To produce a 3D object, one can use a block of material and shape it (by removing material) to a desired form or, one could try to build the desired shape by merging small portions of material. These two techniques can be catalogued as “subtractive process” and “additive process”, respectively.

Although both techniques present their own advantages, one major drawback of the subtractive process is the increase in the quantity of raw material that needs to be used for producing an object.

Additive Manufacturing (AM) or 3D printing refers to a process which uses digital design data to build up a component in layers by depositing material in several layers. It is one of the emerging technologies for the production of three dimensional objects through an additive process (Ford 2014).

The most important additive manufacturing techniques used for polymers are: (1) Fused Deposition Modelling (FDM), (2) Stereo Lithography (SLA) and (3) Selective Laser Sintering (SLS) (Puyvelde 2014). Fused Deposition Modelling will be studied in detail in this work, but firstly these three techniques are briefly explained.

In the **Fused Deposition Modelling** process a filament feedstock is fed into the liquefier using a pinch feed mechanism (Gibson, Rosen and Stucker 2010). This incoming solid filament acts as a plunger/ram to extrude the material through the nozzle (Reddy and Ghosh 2007). These FDM machines use, generally two kinds of materials: a modelling material which constitutes the finished object and a support material which acts as a support for the object, as illustrated in Fig. 1. In a typical FDM process, the extrusion nozzle moves over the building platform in horizontal and vertical directions, "drawing" a cross section of the final product onto the platform. Once a layer is completed, the base is lowered or the extrusion head is raised usually by about 150 micron to make room for the next layer of extruded

material. While the extruded beads/layer of material cools it binds it to the layer beneath it.

The most common material used for FDM process is acrylonitrile butadiene styrene (ABS) (Puyvelde 2014).

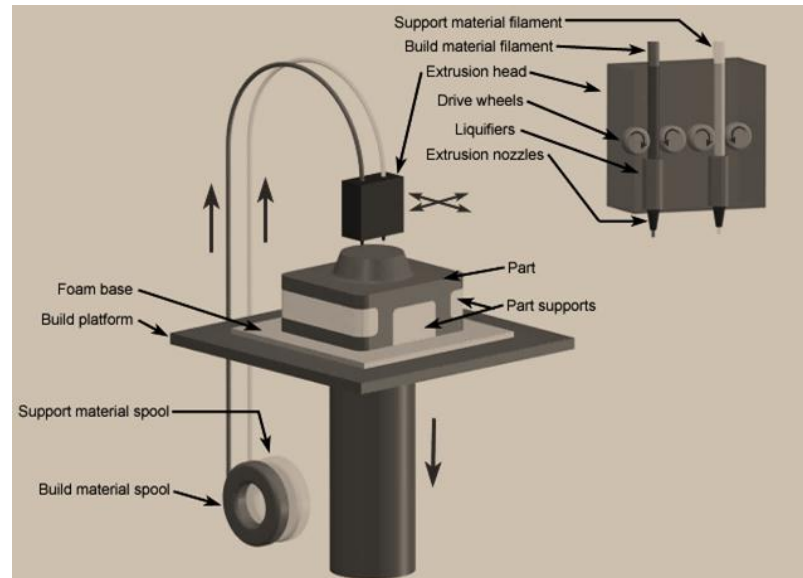


Figure 1 : Fused Deposition Modelling process, adapted from (CustomPartNet 2009)

There are some advantages and disadvantages when using the FDM process. One of the main advantages of the FDM process is its flexibility on the design of complex shape products, especially when soluble supports need to be used. It is a relatively simple system of 3D printing, and even desktop equipment is available for a decent price (Puyvelde 2014). The main drawback of the FDM process is the availability of a limited number of raw materials. The most used feedstock material for FDM process is ABS, which sometimes is blended with polycarbonate (PC) to improve the mechanical properties of the final product (Novakova, Ludmila and Kuric 2012).

Another well-known additive process is the **Stereo Lithography (SL)**. SL is a manufacturing process, which uses a vat of liquid ultraviolet curable photopolymer resin (like for example light-sensitive epoxy resins) with an ultraviolet laser to build the final product layer by layer. For every layer, the laser beam traces a defined cross-sectional pattern of the part on the surface of the liquid resin and the liquid resin cures and joins with the layer below, as illustrated in Fig. 2. After the pattern for one layer has been traced, the SL elevator platform descends by a distance equal to the thickness of a single layer, typically 0.05 mm to 0.15 mm, and the cross section of new layer will be traced. Once the part is build, it will be cleaned in a chemical bath to remove the excess resin, and, sometimes, is subsequently cured in an ultraviolet oven.

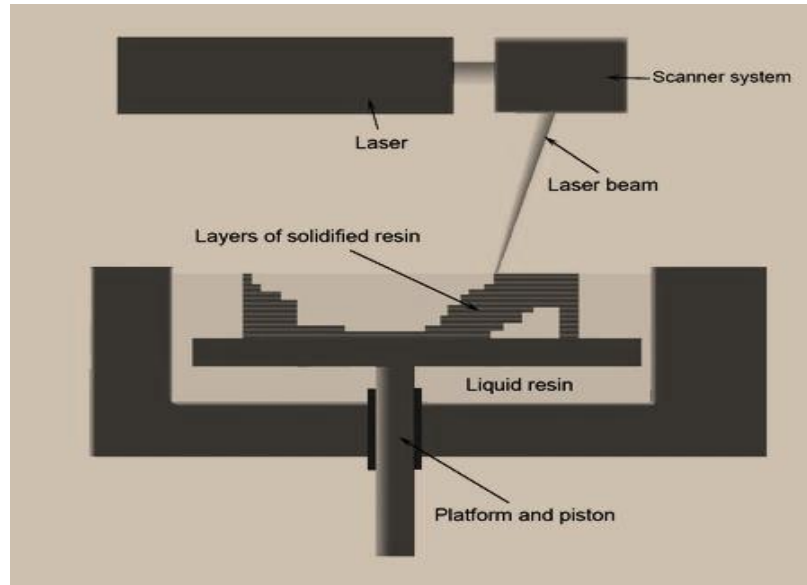


Figure 2 : Stereo Lithography with its components, adapted from (Proto3000 2013)

The main advantage of the Stereo Lithography is the high speed production of parts. Secondly, it is a well-known mature technology (first of the additive manufacturing methodologies). However, the major drawback for Stereo Lithography is its availability for only light-sensitive resins and the use of supports that need to be removed after production, making this technique more expensive (Puyvelde 2014).

A third well-known additive method is the **Selective Laser Sintering (SLS)** process. In this process a laser is used to produce 3D parts that are created layer by layer in a consolidated bed of polymer, as illustrated in Fig. 3. A high power laser (for example, a carbon dioxide laser) fuses small particles of polymer to get the final three dimensional shape of the product (Hopkinson, Hague and Dickens 2006). Computer aided 3D digital description of the part is used to produce the desired cross-section on the surface of the polymer bed, and, once the cross-section in each layer is scanned, the powder bed descends a distance equal to a layer thickness being the new layer scanned on top of the previous layer until the part gets completed. The main advantage of the SLS process over other additive manufacturing processes is that it does not require any support materials because the part is produced in a compact bed of un-sintered material (Puyvelde 2014).

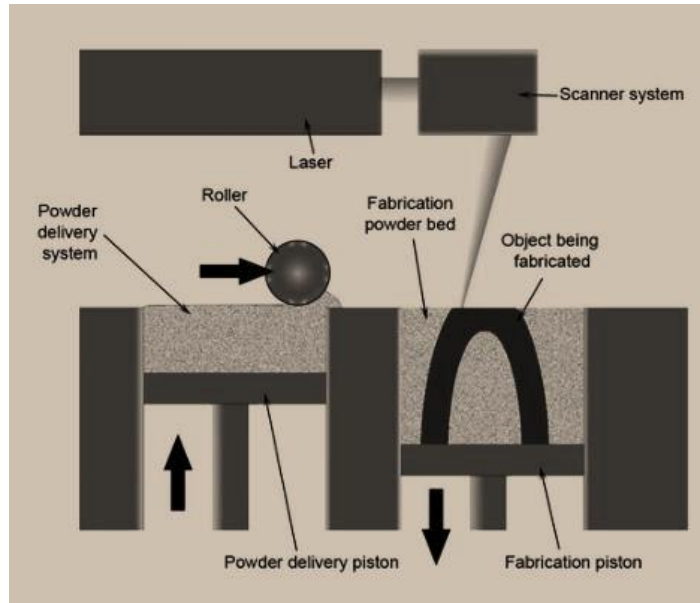


Figure 3 : Selective Laser Sintering and its different parts, adapted from (Treehugger 2015)

The previous text was a brief introduction on the techniques most commonly used for additive manufacturing or 3D-Printing. As mentioned earlier, fused deposition modelling is the chosen method for this work, and therefore, it will be explained in detail in the next chapters.

1.1. Fused Deposition Modelling

Rapid Prototyping is the automated production of a prototype or a final product using computer aided design. The additive manufacturing technology represents the new phase in the evolution of prototyping. The first technique for rapid prototyping become available during 1980s and it was used to produce model and prototype parts. There were more than 20 different rapid prototyping techniques by the end of 1988 being the Fused Deposition Modelling the most common method used for rapid prototyping (Chua, Leong and Lim 2003).

Some quick review on the major milestones in the history of additive manufacturing, tell us that fused deposition modelling was developed by S. Scott Crump in the late 1980s and was commercialized in 1990 by Stratasys in Eden Prairie, Minnesota (Chua, Leong and Lim 2003). In 1984 Charles Hull developed and patented Stereo Lithography. During 1986 Carl Deckard patented Selective Laser Sintering and this technology was made commercial later in 1989. In 2007 Objet Connex launched the first 3D printer that can be used to print an object with multiple materials. Urbee, which is a joint venture between Kor Ecologic and Stratasys, created the first car with a 3D printed body during 2011. During 2013 “Liberator”, the first 3D printed gun was manufactured by Defense Distributed (CEABLOG 2014).

Now, a more detailed review is presented about the fused deposition modelling process, covering the main findings from 1996 onwards.

In 1996, a group of researchers (Agarwala, et al. 1996), made improvements in the fused deposition modelling process for the production of functional ceramic and metal parts. They improved the fused deposition modelling process by eliminating several internal and surface defects that, if not eliminated, would severely limit the structural properties of the final product. They also discussed in detail the other defects present in the earlier processes and proposed several new strategies to eliminate these defects.

During 1997 Yardimci and co-workers (Yardimci, et al. 1997), proposed the complimentary computational models that can be used for the extrusion phase of fused deposition modelling. In their study, dependence of thermal behaviour on nozzle and liquefier design has been studied. Also the influence of the temperature fields near the deposition point is explained, especially for the deposition of multiple material systems.

In 2000 Thomas and Rodríguez (Thomas and Rodríguez 2000), modelled the fracture strength, which develops between the fused deposition extruded filaments, taking into account the wetting and thermally driven diffusion processes. In this work fracture toughness data of fused deposition modelled ABS is used to quantify the proposed model. The result of this study showed that fracture strength mainly develops because of slower cooling rates during solidification, which makes the bonds between the roads stronger.

During 2000, the authors (Venkataraman, et al. 2000), studied the fused deposition of ceramics (FDC). This is a production technique that uses highly filled polymers in filament form as raw material. These feedstock filaments can fail via buckling during their processing, and in this work, a methodology for finding compressive mechanical properties of filaments was developed. The authors also defined the critical limits for which the feedstock material buckles.

In 2002, Sung-Hoon Ahn and his colleagues (Ahn, et al. 2002), explained the critical material properties required for fused deposition modelling raw materials and the effect that FDM process parameters have on anisotropic material properties. The process parameters (raster orientation, air gap, bead width and modelling temperature) were examined and their effects on final product were explained. Experimental results of tensile strength and compressive strength for different ABS products obtained from different raw materials were compared, and they also built many rules for designing FDM parts based on their experimental results.

During 2003 Bellini and Güçeri (Bellini and Güçeri, Mechanical characterization of parts fabricated using fused deposition modeling 2003), concluded that broadening of material choice, improvement of the surface quality, dimensional stability and getting necessary mechanical properties for matching the performance criteria are required when shifting from prototyping to manufacturing of final product. They also

explained the mechanical characterization of products manufactured using fused deposition modelling.

In 2004 Bellehumeur and co-workers (Bellehumeur, et al. 2004), investigated the bond formation between extruded ABS filaments in the fused deposition modelling process. Thermal analysis of the fused deposition modelling process and sintering experiments were performed to explain the dynamics of bond formation between polymer filaments, and, the degree of bonding obtained during filament fused deposition was predicted quantitatively. Their main conclusion suggests that control of the cooling conditions have a strong influence on the mechanical properties of the parts fabricated using the fused deposition modelling process.

During 2004, a group of researchers (Bellini, Guceri and Bertoldi, Liquefier dynamics in fused deposition 2004), described the analysis of liquefier dynamics in order to establish strategies for controlling the flow during the extrusion phase, which is necessary to achieve the good final product in the fused deposition modelling process. They built a mathematical model based on physical assumptions in order to understand the complex phenomena that occurs inside the liquefier. They concluded that the slip between rollers and filament feedstock material are responsible for an error, when sudden changes are applied to the flow rate.

It is well-known that when there are temperature gradients in the fused deposition modelling process, thermal stresses can develop. In 2007, Wang and Jin (Wang, Xi and Jin 2007), analysed the prototype deformation during the fused deposition modelling process. Mathematical modelling of prototype warp deformation was performed, and the effect of influencing factors, such as the stacking section length, the chamber temperature, the number of deposition layers and the material linear shrinkage rate, were explained quantitatively. This work provided some methods for reducing the prototype warp deformation.

In 2008, the authors (Sun, et al. 2008), investigated the mechanism of bond formation between the filaments of extruded polymer in the fused deposition modelling process. They explained that bonding between the extruded filaments is thermally driven and determines the mechanical properties of the final product. Their experiments showed that the manufacturing strategy and the variations in the heat transfer convection coefficients affected the cooling temperature profile and, consequently, the mesostructure of the product and the bonding strength between the extruded filaments. They found that bond formation significantly depends upon the sintering phenomena, and bond formation happens for short interval of time when the temperature of filaments is above the critical sintering temperature.

During 2009 Mostafa Nikzad and his colleagues (Nikzad, et al. 2009), performed the 2D and 3D numerical modelling/analysis of the melt flow behaviour of ABS and Iron composite in the liquefier/print head of fused deposition modelling process using ANSYS FLOTTRAN and CFX finite element packages. They investigated the

basic flow parameters, which include temperature, velocity and pressure drop, and they also produced ABS-iron composite filaments and checked whether they can be used for current fused deposition modelling machines. The result of their work provided good information for building melt flow models for metal plastic composites, and they also optimized FDM parameters for better quality of such composites.

In 2010 Liang and Tian (Ji and Zhou 2010), developed a 3D transient thermal finite element model for fused deposition modelling of ABS considering temperature dependent thermal conductivity and heat capacity. Their main results were that temperature field distribution is like an ellipse and the highest temperature gradient occurs near the edge of the deposited part.

During 2012 Halidi and Abdullah (Halidi and Abdullah 2012), showed that the presence of moisture affects the FDM process of ABS. Basically, they concluded that moisture affects the physical, morphological and thermal stability changes of the polymer. Also, experiments were conducted to check if these changes may have caused the blockage of the nozzle. They concluded that the blockage of the nozzle was due to the morphological and thermal stability changes of the ABS when it is exposed to moisture.

1.2. Motivation/ Objectives

- One of the motivations of this work is to study the rheological properties of acrylonitrile butadiene styrene, in order to assess the suitability of different grades (samples) of ABS to be used as feedstock material in the fused deposition modelling process.
- ABS is one of the most used feedstock materials in the fused deposition modelling process. It is used in the form of filaments and it is more expensive than the ABS available in the form of pellets. In some cases the difference is very high (of the order of 15 to 100 times higher). Therefore, the main motivation/objective of this work comes from this economic factor. Being the objective to check scientifically if there is any reason justifying this difference in prices. Also, it is intended to check if there are some major requirements/differences for the ABS grades, when they are to be used in the fused deposition modelling process.

1.3. Route to Objectives

- The first step in this work is to do the rheological characterization of different grades (samples) of ABS available in the form of pellets or filaments. The rheology of these materials is not very well characterized yet in the literature and the rheology data obtained will also be the key to detect differences between the various ABS grades (samples) used.

- The glass transition temperature of different ABS grades (samples) will be measured.
- 3D printing of different grades (samples) of ABS in predefined shape specimens.
- Lastly, these specimens will be characterized mechanically and optically. The specimens will be tested for mechanical properties via flexural testing, and, optical microscopy will be used to check the sintering and adhesion achieved for different ABS feedstock materials.
- Finally numerical and analytical modelling of the flow of the polymer in the nozzle of the fused deposition modelling machine will be performed, in order to check how different grades (samples) of ABS behave during 3D printing.

1.4. Thesis Structure

In the first chapter there is an introduction to Additive Manufacturing process, covering the state of the art on the FDM process. This chapter also explains the motivation/objectives and route towards objectives. The second chapter encompasses the theoretical description of materials and of all the different methods used in this work. The third chapter covers the basic constitutive equations used for viscous viscoelastic numerical modelling. In the fourth chapter, experimental setups and the results of rheological testing, 3D-printing using different samples of ABS and characterization of the printed specimens (mechanical and optical) is presented. This chapter also includes a detailed discussion on all the obtained results. The last chapter of the thesis is devoted to the numerical modelling of the flow of different grades of ABS in the nozzle of the fused deposition modelling machine. The thesis ends with the conclusions, and, a brief description of the proposed future work is presented.

Chapter 2

2. Materials and Methods

2.1. Materials

Polymers are made up of very large number of repeating units (monomers), and, their molecular mass varies from 10000 to 1000000 grams/mole, which is extremely high when compared to normal low molecular weight materials e.g benzene 78 g/mol and glucose 180 g/mol. The polymer molecules are in the form of long chains and those chains can be branched, linear, or even form a network (that can be temporary because of physical entanglements or permanent due to chemical crosslink between the molecules (Fried 2014)).

Polymers can be classified based on their origin: (1) natural, (2) semi synthetic and (3) synthetic. Natural polymers are abundantly present in vegetables and animal tissues e.g cellulose, wool and silk. Semi-synthetic polymers are partly from natural origin but they have been chemically modified into half synthetic polymers. Leather and technical rubber are common examples of semi-synthetic polymers. Lastly, synthetic polymers are the ones in which the network or the chains of the polymers are built from low molecular mass substances (monomers) in a chemical process. The low molecular mass components are mostly organic monomers, and, these monomers are obtained from fossil fuels. Some examples of synthetic polymers are polyethylene (PE), acrylonitrile butadiene styrene, and, polyether ether ketone (PEEK) (Fried 2014).

The other way of classifying the polymers is based on their structure. There are two main categories: (1) single chain and (2) network structure polymers. The first type, single chain polymers, as illustrated in Fig. 4, are mostly linear polymers, although these chains can be branched. The stiffness of such polymers is relatively low (Van der Vegt 2006).



Figure 4 : Linear Polymer with Entanglements, adapted from (W.J. Briels 1998)

In the network structure polymers, as shown in Fig. 5, molecular chains are strongly connected by primary chemical links, and flow of the network polymer is not possible as it is hindered by permanent chemical links (Van der Vegt 2006).



Figure 5 : Cross-linked Polymer, adapted from (Donna Narsavage-Heald n.d.)

Now, based on the above structural features, polymers are divided in three main categories of practical (industrial) importance: (1) Thermoplastic (2) Thermosets and (3) Elastomers, as illustrated in Fig. 6.



Figure 6 : Different types of Polymers, where, a small bead represents the monomer unit. Adapted from (Adhesivesandglues.com 2012)

Thermoplastic: These are non-cross-linked systems, which flow at high temperatures, and, when cooled return to solid state. They can take two different forms of structures, amorphous or crystalline structures (as shown in Fig. 7) depending upon the degree of the intermolecular interactions that occur between the polymer chains (Fried 2014).

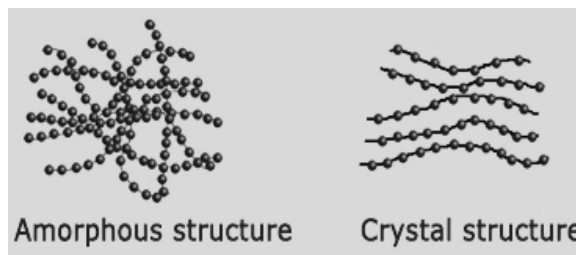


Figure 7 : Amorphous and Crystalline structures, where small beads represent the monomer units. Adapted from (Adhesivesandglues.com 2012)

Thermosets: These materials are made of polymer chains that are linked together by chemical bonds, resulting in a highly cross-linked polymer structure, as illustrated in Fig. 6 (Fried 2014). They have high mechanical and physical strength as compared to thermoplastics or elastomers. The main limitation of thermosets is their poor

elasticity and elongation properties because of highly cross-linked structures (Van der Vegt 2006).

Elastomers: In these materials, polymer chains have slightly cross-linked (network) structure, as shown in Fig. 6. They are capable of returning to their original shapes when they are released after stretching (Van der Vegt 2006).

There are some other types of polymers, which are made up of more than one type of repeating units. They are mainly copolymers, as described below,

Copolymers: There are some properties of polymers that are obtained by linking more than one type of monomer or repeating units during polymerization (a reaction in which monomers react to form long chain polymers). When two different monomers or repeating units are polymerized to obtain desirable properties, these polymers are called copolymers (Fried 2014).

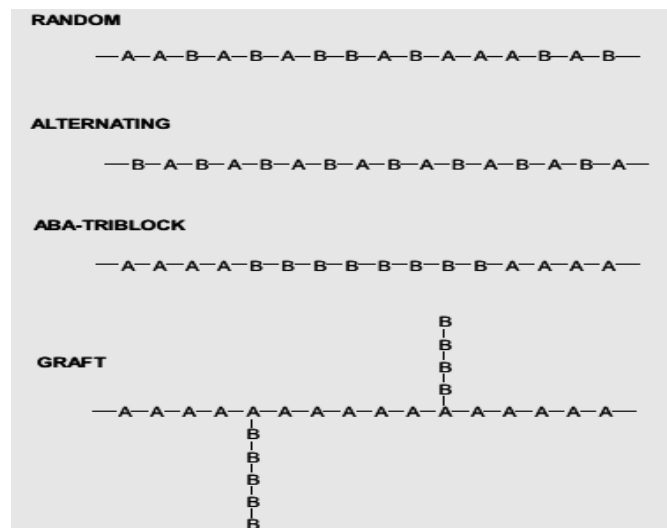


Figure 8 : Different structures of copolymers, where A and B are the different monomer units, adapted from (Fried 2014)

The linking pattern of different monomers in copolymers can be totally random or may be perfectly alternating, as illustrated in Fig. 8. Those copolymers that possess a long block of one type of monomer (A) followed by a block of another type of monomer (B) can be obtained under special reaction (polymerization). These copolymers are called block-copolymers, as shown in Fig. 8. An example of commercially important block copolymer is styrene butadiene styrene (SBS). Graft copolymerization usually results in high impact strength polymer e.g acrylonitrile butadiene styrene (ABS) (Fried 2014).

Now, a brief description of ABS will be presented, as this is the material used as feedstock in this work.

Acrylonitrile Butadiene Styrene is a thermoplastic copolymer polymer, as shown in Fig. 9, having amorphous structure. It is a terpolymer (terpolymer is a copolymer

comprised of three different monomers), which is produced by polymerizing styrene and acrylonitrile in the presence of polybutadiene. The polymerization results into a long chain of polybutadiene with shorter chains of poly (styrene-co-acrylonitrile). The main advantage of ABS is that this material combines the strength and rigidity of the acrylonitrile and styrene polymers with the toughness of the polybutadiene rubber.

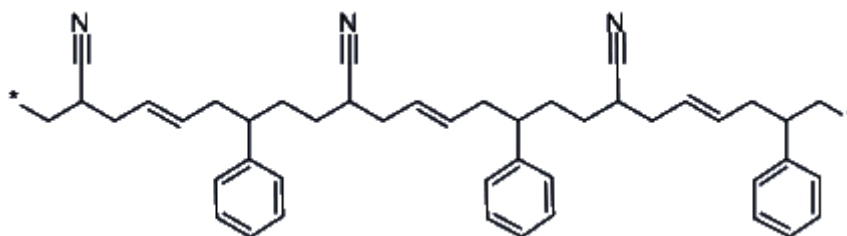


Figure 9 : Structural formula of ABS. Adapted from (Chemical Book 2010)

The most important mechanical properties of ABS are toughness and impact strength, and, it is widely used in applications where impact resistance and structural strength are necessary. ABS has excellent dimensional stability. That is why it is ideal for pre-production of rapid prototypes that can accurately predict performance of final products (RedEye 2015).

2.2. Basic Concepts: Rheology and Rheometry

Rheology is the science of flow and deformation of matter under the effect of an applied force. The term rheology comes from the ancient Greek word *rheos* that means flow and *logia* that means the science/the study. It is normally used to describe the consistency of different material systems, with two behaviour components, viscous and elastic. Viscosity explains the resistance to flow or the friction between different layers during the flow, and, elasticity describes the stickiness or structure of the material system. The other use of rheology is that it helps us predicting the behaviour of the material in processing, and, the performance of the final product (Schowalter 1978).

In order to compare different materials, we have to define properties, such as, for example, the resistance of the material to flow. These properties can be measured with the help of rheometry.

Rheometry explains the experimental techniques that are used to determine the rheological properties of the materials to be studied. The main function of rheometry is to quantify the rheological material parameters which are practically important. The instruments that are used to measure the rheological properties of the materials are rheometers (Shenoy and Saini 1996). Their working principle is one of the following two:

1. One can apply deformation on the material and measure the force generated
2. One can apply force on the material and in response measure the deformation

There are different geometries that are used in the rheometers, and, certain calculations are performed to convert force/deformation to the corresponding stresses and strains, which then can be used to calculate material parameters (Shenoy and Saini 1996).

There are two main categories of rheometers (1) **Rotational rheometers** and (2) **Capillary rheometers**.

Rotational rheometers are used in two main modes: controlled rate and controlled stress. For the controlled rate rheometers, the material, which has to be characterized, is placed between two plates and then one of the two plates rotates at constant speed. The torsional force it produces on the other plate is measured. So, in this case, speed (strain rate) is the independent variable and torque (stress) is the dependent variable, as shown in Fig. 10, (Tabilo-Munizaga and Barbosa-Canovas 2005).

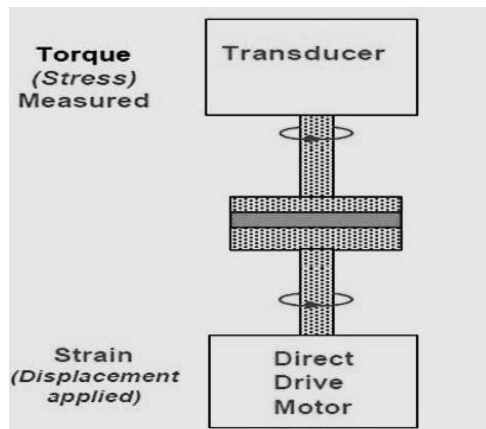


Figure 10 : Strain controlled rheometer. Adapted from (Jeffrey Gotro 2014)

For controlled stress rheometers the displacement or rotational speed (strain rate) is measured on the plate in response of a predefined torque, which is applied on the same plate, as shown in Fig. 11.

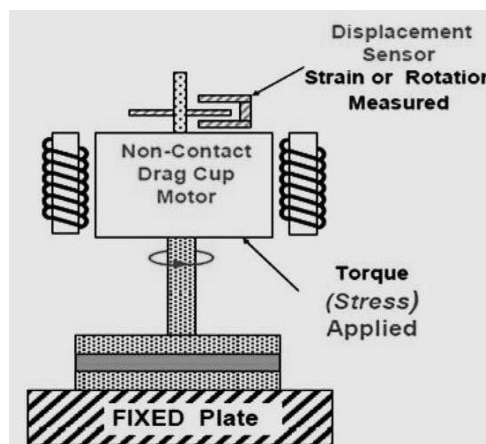


Figure 11 : Stress controlled rheometer. Adapted from (Jeffrey Gotro 2014)

Now, let us review the different geometries that are used in rotational rheometers. Most common geometries are cone and plate, concentric cylinder, parallel plate and torsion rectangular, as shown in Fig. 12.

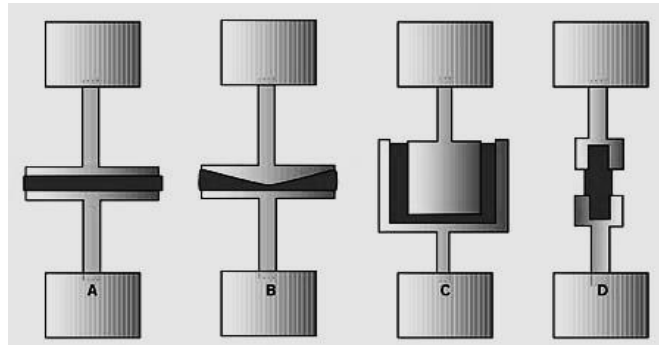


Figure 12 : Rotational rheometers (A) Parallel plate (B) Cone and plate (C) Concentric cylinder and (D) Torsion rectangular. Adapted from (John R. Schrei 2002)

These different geometries are used for different types of materials. Concentric cylinder geometry is used for very low to medium viscosity samples. It cannot be used for pastes because there can be air bubble formation and it will affect the results. The materials with very low to high viscosity are used in cone and plate geometry. This geometry is basically used for liquid samples it has a limitation that it can be used for dispersions; only when the particle size is less than 5 micro meter. Parallel plate geometry is used for very low viscosity liquids to soft solids. It is used for gels, pastes, soft solids and polymer melts. Torsion rectangular rheometer is used for very soft to very rigid solids (Shenoy and Saini 1996).

As mentioned earlier, the second main category of the rheometers is capillary rheometry. Its basic application is in the polymer processing industry, but it is also relevant for many other processes for example high speed coating and printing applications. These capillary rheometers (shown in Fig. 13) are based on controlled extrusion of the material through a circular die (capillary), where the material flows. Deformation properties are characterized using conditions of high force/pressure, high shear rate and high temperature.

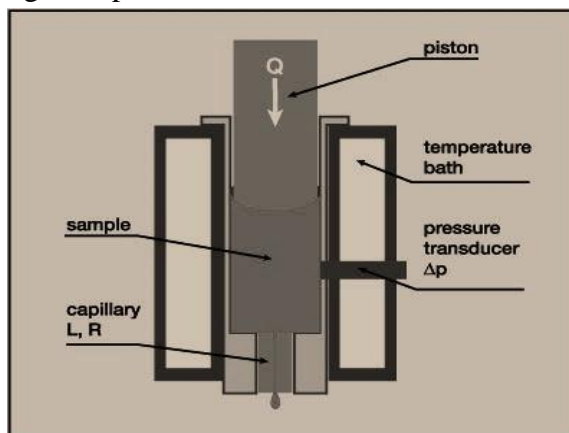


Figure 13 : Capillary rheometer and its basic parts. Adapted from (ASI adhesives & sealants 2003)

Generally, the material is pushed from a reservoir into a capillary at constant velocity and pressure drop is measured. The measured pressure drop has entrance and exit effects. Therefore, a correction in the measured pressure drop is necessary to eliminate the entrance/exit pressure drop effects. Bagley correction is done to get the real value of pressure drop. It considers that the extra pressure drop due to end effects can be represented by an equivalent extra length of the die. So, experiments with two to four dies of same diameter, but different lengths, are performed keeping the piston speed constant. In this way end effects can be eliminated and true shear stress can be found (Shenoy and Saini 1996).

Some of the advantages of capillary rheometers are:

1. Characterization at high shear rates e.g (10^0 to 10^5 s^{-1});
2. It can provide an estimation of the extensional behaviour of the sample, assuming the validity of the Cogswell analysis (Padmanabhan and Christopher 1997).
3. Detection of the onset of rheological flow defects is possible.

This technique also has some limitations:

1. Corrections of the data are necessary;
2. Measurement of the elastic functions is not easy;
3. Data precision is affected by viscous dissipation and flow instabilities.

The previously described rotational and capillary rheometers are those applicable for shear flows, but there are some polymer processing techniques where elongational (extensional) flows are important e.g blow moulding and fiber spinning. These flows are different from shear ones, so they must be treated in a different way, to get, for example, extensional viscosity (defined as resistance to flow when the stress is applied to elongate the material). Generally, steady state extensional viscosity is very difficult to measure because both extensional rate and stress must be constant. A steady extensional rate can be obtained if the ends of the sample are pulled apart at a rate that increases exponentially with time (Shenoy and Saini 1996). The other important thing is that force should remain constant for steady state to be achieved but most of the times sample breaks before steady state can be achieved or the equipment limits exceeds (Shenoy and Saini 1996). However, several methods were attempted and are available for measuring extensional viscosity. Some of them are Meissner elongational rheometer, Sentmanat elongational rheometer and Cross-Slot elongational rheometer.

There are different rheological tests that can be performed in order to characterize different materials and these are mentioned in Table. 1.

Table 1: Different rheological tests used to characterize the rheological behaviour of materials

Test	Rheometer	Rheological outputs
SAOS* frequency sweep	Rotational (Cone and plate or Parallel plate geometry)	$G'(\omega)$, $G''(\omega)$ Dynamic moduli (spectrum of relaxation time), $\eta'(\omega)$, $\eta''(\omega)$ Dynamic (complex) viscosity
Step shear rate	Rotational	$\eta(\dot{\gamma}, t)$ Zero shear viscosity and Shear thinning
Shear rate sweep	Capillary	$\eta(\dot{\gamma})$ Shear thinning
Step extensional rate	Extensional	$\eta(\dot{\epsilon}, t)$ Shear hardening

*SAOS = Small amplitude oscillatory shear

2.3. Thermal Characterization/Analysis

In case of thermoplastic polymers, when thermal analysis is done, we are concerned with the two important transition temperatures:

1. Glass Transition Temperature (T_g)
2. Melting Temperature (T_m)

Glass Transition Temperature (T_g): This temperature is important in case of amorphous polymers and for the amorphous portion of semi-crystalline polymers, but, the crystalline portion of semi-crystalline polymer remains unaffected during glass transition.

When the polymer is at low temperature its amorphous regions are in a glassy state. In this glassy state the molecules of the polymer are frozen at their positions and they possess only vibrational motions and do not have any long or short range segmental motion. In this state the polymers are hard, rigid and brittle.

When the polymer melt is cooled from the liquid state, it becomes more viscous and flows less readily. As the temperature is reduced low enough (glass transition temperature), the polymer becomes a relatively hard and elastic material (glassy state), as illustrated in Fig. 14. When polymers are above their glass transition temperature they possess short and long range segmental motions, and they are in the rubbery state (Gonzalez-Gutierrez 2015).

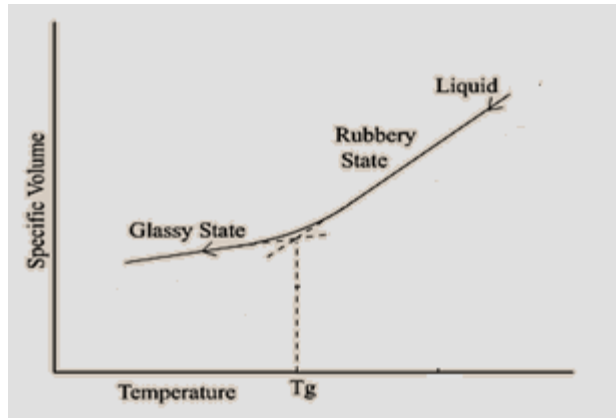


Figure 14 : Glass transition temperature of an amorphous polymer. Adapted from (Gonzalez-Gutierrez 2015)

An important concept when talking about glass transition temperature, is, the free volume. As the temperature of the polymer melt is lowered, the free volume will be reduced until eventually there will not be enough free volume to allow segmental motions to take place. The temperature at which this happens corresponds to T_g , as below this temperature the polymer is effectively frozen (Goderis 2014).

Melt Temperature (T_m): In case of semi-crystalline polymers, when they are heated there comes a temperature at which the crystals of the polymers melt, as illustrated in Fig. 15, and the polymer can flow easily. An important thing to be looked in the case of semi-crystalline polymers is that the degradation temperature for semi-crystalline materials is not much higher than their melting temperature.

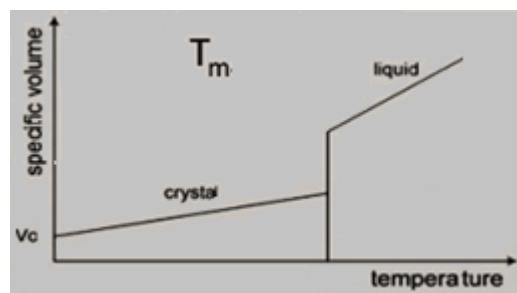


Figure 15 : Melting transition of crystalline polymers. Adapted from (Gonzalez-Gutierrez 2015)

In order to measure and obtain these temperatures, some equipment needs to be used. In our case we have used the differential scanning calorimetry.

Differential Scanning Calorimetry (DSC): It is the most common technique used for thermal analysis (Fig. 16). Differential scanning calorimetry is used for thermal analysis/characterization of thermoplastic material. It can also be used to measure melting temperature and heat of fusion of metal alloys, to measure the glass transition temperature, melting temperature and heat capacity of the thermoplastics (O'neill 1964).

The basic working principle of the DSC is based on the fact that it measures the differences in the amount of heat required to increase or decrease the temperature of sample and reference pan, as a function of temperature. The sample which is placed in the sample pan undergoes a physical transformation such as phase transitions. During this phase transition different amount of heat will flow to the sample pan as compared to the reference pan, and so, the DSC measures this different amount of heat absorbed or released during such phase transitions.

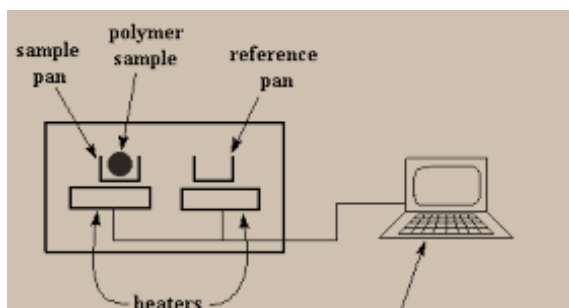


Figure 16 : Differential scanning calorimetry, sample pan and reference pan.

There are two commonly used DSC systems, (1) Heat-flux DSC and (2) Power-compensation DSC, as shown in Fig. 17. In heat-flux DSC, a low resistance heat flow path (metal disc) is used to connect the sample and the reference pan. This whole assembly is closed in a single furnace, as illustrated in Fig. 17 a. The different temperature of the sample pan relative to the reference pan is caused by enthalpy or heat capacity changes in the sample, and it results in very small heat flow (Bhadeshia 2002).

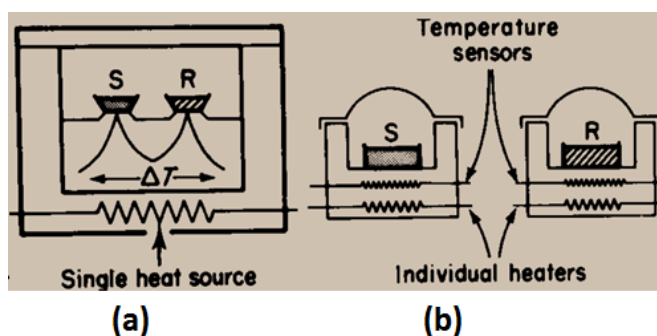


Figure 17 : Two DSC systems (a) Heat flux DSC, (b) Power-compensation DSC, adapted from (Bhadeshia 2002)

In the power-compensation DSC type two separate identical furnaces (as illustrated in Fig. 17 b) are used to control the temperatures of the sample and the reference pan. The power input of the two furnaces is varied to make the temperature of the sample and reference pan identical. The energy used to do so, quantitatively represents the enthalpy or heat capacity changes in the sample relative to the reference (Bhadeshia 2002).

2.4. Production of Specimens

2.4.1. Extrusion of Filament

Extrusion is the most commonly and widely used polymer processing technique. A common extrusion process is illustrated in Fig. 18. There is a hopper attached to the barrel of extrusion machine which acts as the feeding point for plastic pellets or any other additives that needs to be added in order to get the final product. When material enters the extruder, it is pushed forward along the extruder barrel with the help of a rotating screw. As the polymer beads move forward along the barrel, the combination of external heating with the heating resulting from friction on the barrel walls melts the polymer beads. Once the material is completely melted, the screw further conveys the molten plastic until it exits the extruder barrel through a shaping tool (die). This shaping tool imparts a predefined shape to the molten plastic, and the extruded profile is immediately cooled down with the help of, for example, a water bath. The output of the extruder is termed as extrudate (Strong 2005).

The extrudate is pulled at a constant rate with the help of pull roller that acts as auxiliary equipment. There can also be some other auxiliary equipment for cutting the part in an exact required length, for coiling, stacking and packaging of the product for shipment.

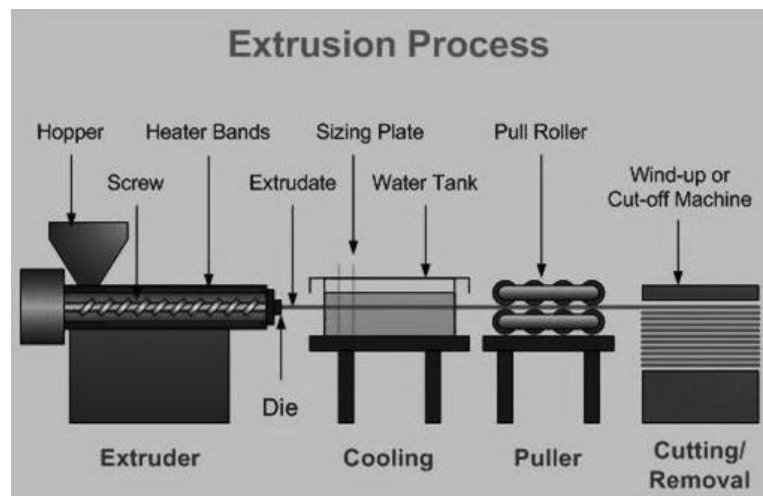


Figure 18 : Extrusion line including auxiliary equipment's (cooling system, puller and cutting system), adapted from (rediff blogs 2012)

It is the least expensive method to achieve high production volumes of plastic parts as it is a continuous process. Although, one of the drawbacks of the extrusion process is that it can only produce parts with constant cross section (Strong, 2005).

There are different samples (grades) of ABS that are going to be used in this work, as illustrated in Table 2 in Chapter 4. One of these samples; sample 1, is in the form of pellets. So, the extrusion process was used for producing filaments of sample 1,

because, only filaments can be used as feedstock material in fused deposition modelling.

In order to produce these filaments, the extrusion temperature was set to 190°C for the feeding section and 200 °C along the rest of the barrel. The production of the filaments was carefully controlled in order to obtain a diameter between 1.7 to 1.8 mm, as requested by the 3D printing equipment used. The rolls puller system was used to control the diameter of the filament precisely.

2.4.2. 3D Printing Process

In this work, FDM is the chosen process for printing the specimens. The process was briefly explained in the introduction chapter. In this section the key features and components of the FDM process will be explained in detail. These key components include the material feeding mechanism, liquefier and print head, gantry, build surface and build environment, as illustrated in Fig. 19.

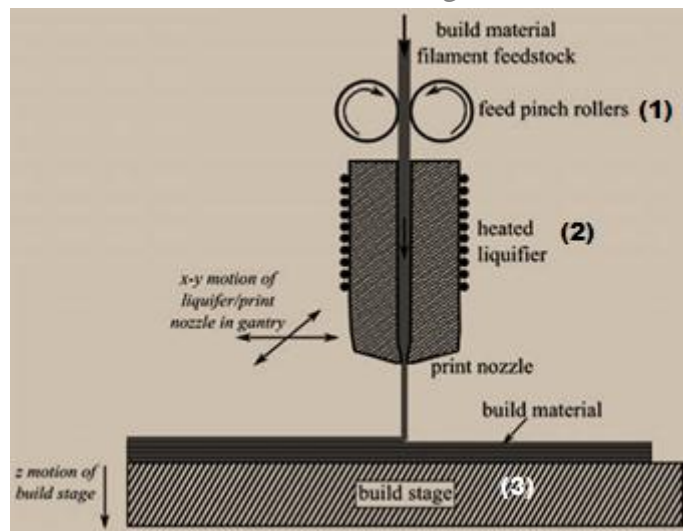


Figure 19 : FDM process and its components; (1) Feed pinch rollers, (2) Liquefier/print head and (3) Build surface

Feeding Mechanism: In conventional polymer processing techniques feedstock material is in the form of pellets but in the FDM process the typical feedstock material is in the form of filaments of varying diameters from 1.5 to 3 mm. These feedstock materials are available in different options. For the small scale systems the materials can be found in the form of loose coils while they can be found in the form of a cartridge for large scale manufacturing systems.

A pinch roll feed mechanism is used to push the filament feedstock (with the help of a motor), as illustrated in Fig. 19. The surfaces of the rolls have grooves or teeth in order to create sufficient friction between the rolls and filament to feed the liquifier at a constant rate (without slippage). Note that the compression force of the rolls leaves a minor tooth mark on the filament, but, it should be designed and controlled carefully so that it does not crush the filament (Agarwala, et al. 1996). Also, the presence of moisture in feedstock filaments can lead towards significant

problems in the FDM process as it will vaporize when it passes through the nozzle. If moisture is present in significant quantities it can cause blockage of the nozzle and the formation of bubbles in the printed samples (Halidi and Abdullah 2012). Feed stock materials available in the form of cartridge can keep the filaments dry more efficiently than simple feedstock in the form of coils.

Liquefier/print head and gantry: One of the key parts of the fused deposition modelling machine is the liquefier. It is a metal block where the filament feedstock melts, as illustrated in Fig. 19. The heating mechanism used by the liquefier to melt the feedstock is resistive heating. It is designed in such a way that it maintains uniform temperature throughout the liquefier. However, the generation of the melt in the liquefier depends on the feed rate of the material and also on the heat flux (normally the raw materials for fused deposition modelling process are amorphous polymers and they do not have defined sharp melting temperature).

The increase in temperature will lead to a decrease in the pressure drop, due to the reduction of viscosity. This reduction of viscosity will also improve the sintering and adhesion behaviour between the extruded roads or filaments.

The only drawback of using high temperature is the possibility of polymer degradation. If the polymer degrades, it can leave residue material inside the liquefier which will affect the performance of the feeding mechanism (Gibson, Rosen and Stucker 2010). Lastly, this liquefier/print head is mounted on the gantry which enables the motion of liquefier/print head in x-y plane.

Build surface: : Once the material gets melted inside the liquefier/print head then it is pushed out of the nozzle and extruded on a horizontal base surface that can move in the vertical direction (in the z-direction), as illustrated in Fig. 19. So this motion, in combination with the liquefier/print head motion (in the x-y plane), allows 3D parts to be manufactured, as shown in Fig. 19.

The temperature of the build surface is an important parameter, and, it should be controlled carefully. The temperature should be high enough so that the extruded filaments can adhere to the surface, but not so high that the part removal becomes difficult when the printing is finished.

Normally there are thermal gradients present in the printed parts as they are produced layer by layer on the build surface. If these thermal gradients are large they can distort the structure of the final product (Wang, Xi and Jin 2007).

The parts produced with the FDM process have a ridged and rough surface (inherent to the process), but this surface can be made smooth by using one of these two methods: (1) chemical smoothing and (2) mechanical smoothing (Gibson, Rosen and Stucker 2010). Also, surface coatings can be used to achieve the desired part finish.

2.5. Characterization of Specimens

Mechanical Testing: There are different mechanical properties of plastics such as the elastic modulus, Poisson's ratio, compressive modulus and flexural modulus. These mechanical properties of the specimens can be characterized with the help of different mechanical tests. The most common type of test used to measure the mechanical properties of a material is the tensile test.

The test used in this thesis is the **Flexural Test** that measures the force required to bend the beam under a load which is applied at three different points, as shown in Fig. 20. During flexural testing, the specimen (beam) is supported at two ends and the load is applied at the center of the beam by the loading nose, producing a three point bending at a defined rate.

The flexural test is used to determine the ability of the specimen to resist the deformation under bending loads, and, during the flexural test the beam is under compressive stress at the concave surface and tensile stress at the convex surface (MatWeb 2014).

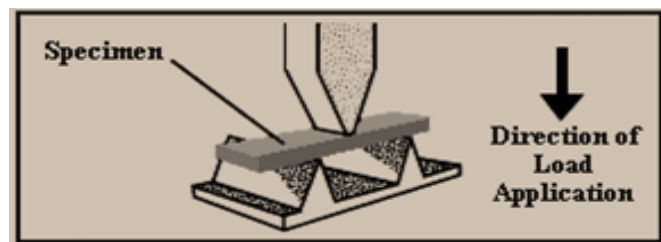


Figure 20 : Flexural testing, three point bending test. Adapted from (MatWeb 2014)

Some important parameters to be considered during flexural testing are length of the specimen, speed of the loading, and the maximum deflection. These parameters depend upon the thickness of the specimen and are defined differently by ASTM and ISO standards (MatWeb 2014).

Chapter 3

3. Basic concepts: Equations and Modelling

There are two major steps when modelling physical phenomena. The first step is to find the mathematical model that reproduces what we are trying to model, and the second step is to solve the mathematical equations.

These equations should be sophisticated enough so that they can predict well the physical phenomena ranging from small scales to big scales. The main problem is that to obtain such good models, complex mathematics needs to be used, thus making difficult the analytical solution of the models. Therefore, a numerical procedure must be adopted. We can also try to find analytical solutions for specific fluids and geometries, but in this way the model will only be adequate to describe simple systems.

In the next two subsections we present the models used to model the fluid flow in the liquefier. We will start talking about the Newtonian and inelastic non-Newtonian fluids, and then, the viscoelastic models will be discussed.

3.1. Newtonian and Generalized Newtonian Fluids

Non-Newtonian inelastic, incompressible fluids are governed by the continuity equation

$$\nabla \cdot \mathbf{u} = 0, \quad (1)$$

and the momentum equation,

$$\frac{\partial(\rho \mathbf{u})}{\partial t} + \rho \nabla \cdot \mathbf{u} \mathbf{u} = -\nabla p + \nabla \cdot \boldsymbol{\tau}. \quad (2)$$

In Eq. 2, \mathbf{u} is the velocity vector, p is the pressure, $\boldsymbol{\tau}$ is the deviatoric stress tensor and the gravity contribution is incorporated in the pressure. All equations are written in a coordinate free form. The stress tensor obeys the following law for generalized Newtonian fluids,

$$\boldsymbol{\tau} = 2\eta(\dot{\gamma}) \mathbf{D} \quad (3)$$

with the rate of strain tensor \mathbf{D} given by,

$$\mathbf{D} = \frac{1}{2}([\nabla \mathbf{u}] + [\nabla \mathbf{u}]^T), \quad (4)$$

and $\eta(\dot{\gamma})$ representing the fluid viscosity function.

For the case where viscosity is constant, $\eta(\dot{\gamma}) = \mu$, we are in the presence of a Newtonian fluid. When the viscosity varies (for example, with the shear rate) it means the fluid is no more Newtonian, and it is called non-Newtonian.

Depending on how viscosity changes with time, the flow behaviour is characterized as thixotropic (time thinning, i.e. viscosity decreases with time) or rheopectic (time thickening, i.e. viscosity increases with time). Thixotropic fluids are quite common (e.g yogurt and paint) while rheopectic fluids (e.g gypsum paste) are very rare.

From experiments, it is well known that the viscosity of some materials depends on the shear rate. Depending on how viscosity changes with shear rate the flow behaviour is characterized as:

- Shear thinning: the viscosity decreases with increased shear rate;
- Shear thickening: the viscosity increases with increased shear rate;
- Plastic: exhibits a so-called yield stress value, i.e. a certain stress must be applied before flow occurs.

Examples of shear thinning fluids are, polymer melts, paints, shampoo and ketchup. Examples of shear thickening fluids are wet sand and suspensions. Examples of plastic fluids are tooth paste and hand cream.

Based on this, several empirical models were proposed in the literature for the viscosity dependence on the second invariant of the stress tensor (which coincides with the shear rate for a simple shear deformation), and we now briefly explain some of these models.

The power law model is given by

$$\eta(\dot{\gamma}) = a\dot{\gamma}^{n-1} \quad (5)$$

where a and n ($n=1$, Newtonian fluid; $0 < n < 1$, shear thinning; $n > 1$, shear thickening) are its parameters. This model presents some limitations, such as, for example, the inexistence of a Newtonian plateau. Therefore, more sophisticated models were developed, such as the Carreau model that already accounts for these features of the Non-Newtonian fluids:

$$\eta(\dot{\gamma}) = \mu_{\infty} + (\mu_0 - \mu_{\infty}) \left[1 - (\lambda \dot{\gamma})^2 \right]^{\frac{m-1}{2}} \quad (6)$$

Here, μ_{∞} , μ_0 , λ , and m are constant parameters which are determined by experimental investigations. For both models $\dot{\gamma} = \sqrt{-4\Pi_D}$, with Π_D the second invariant of the rate of strain tensor.

These models are also known as “generalized Newtonian”. Because they only describe well simple shear flows, they are not suitable for flows where the elastic effects are relevant (for example extensional flows), where new constitutive equations must be used, such as, viscoelastic models.

3.2. Viscoelastic Fluids

The key features of viscoelastic fluids, is the existence of relaxation and retardation times. When we apply a strain to a Newtonian fluid the response is

instantaneous (the relaxation time is zero or almost zero). On the other hand, if we have a viscoelastic fluid, the response will have a delay (the relaxation time is different from zero).

Maxwell proposed a viscoelastic model that couples the two components of the viscoelastic fluid behaviour (elasticity and viscosity). To represent the mechanical equivalent of this model we can assume a spring (elasticity) connected to a dashpot (viscosity), with both objects subject to the same stress, as shown in Fig. 21.

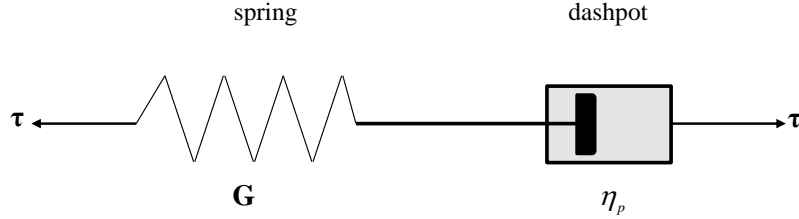


Figure 21 : Representation of the viscoelastic behaviour with a spring and dashpot

For quick deformations the fluid behaves as a Hookean elastic solid with modulus of elasticity G ; for slow deformations the fluid behaves as a Newtonian fluid. For solids, the stress is given by a constant (G) times the deformation (strain) $\tau = G\gamma_e$, while for a liquid, the deformation can be infinite so the measure “deformation” is of no use. Consequently, the rate of deformation ($\dot{\gamma}_v$) is used instead, ($\tau = \eta_p \dot{\gamma}_v$). The total rate of deformation is given by $\dot{\gamma} = \dot{\gamma}_e + \dot{\gamma}_v$ meaning that,

$$\frac{1}{G} \frac{d\tau}{dt} + \frac{\tau}{\eta_p} = \dot{\gamma} \quad (7)$$

With some algebra and using tensor variables, we arrive at the Maxwell model,

$$\boldsymbol{\tau} + \lambda \frac{\partial \boldsymbol{\tau}}{\partial t} = 2\eta D \quad (8)$$

that can be generalized in order to become frame invariant, resulting in the Upper Convected Maxwell model,

$$\boldsymbol{\tau} + \lambda \overset{\vee}{\boldsymbol{\tau}} = 2\eta D \quad \text{with} \quad \overset{\vee}{\boldsymbol{\tau}} = \frac{\partial \boldsymbol{\tau}}{\partial t} + \mathbf{u} \cdot \nabla \boldsymbol{\tau} - [(\nabla \mathbf{u})^T \cdot \boldsymbol{\tau}] - [\boldsymbol{\tau} \cdot \nabla \mathbf{u}] \quad (9)$$

Several other models exist in the literature, and a possible way to construct new models could be the use of different combination of springs and dashpots, as shown in Fig. 22.

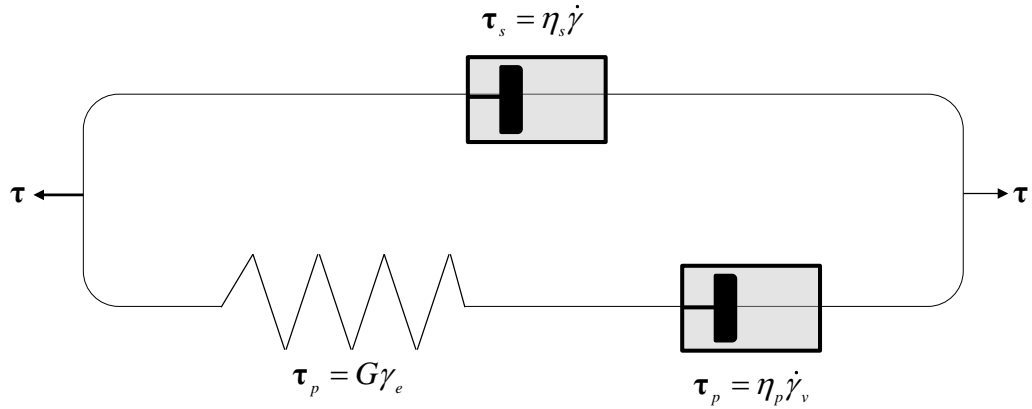


Figure 22 : Representation of the viscoelastic behaviour with springs and dashpots (different combinations)

Not all constitutive equations are derived from combinations of spring and dashpots. Some of the models also originate from molecular or network theories.

We now present two well-known viscoelastic models, the PTT model, developed by Phan-Thien and Tanner (Phan-Thien 1978), (Thien and Roger 1977), and the Giesekus model (Giesekus 1982).

The **PTT** model is described by the equation,

$$f(tr[\boldsymbol{\tau}])\boldsymbol{\tau} + \lambda \left(\frac{\partial \boldsymbol{\tau}}{\partial t} + \mathbf{u} \cdot \nabla \boldsymbol{\tau} - [(\nabla \mathbf{u})^T \cdot \boldsymbol{\tau} + \boldsymbol{\tau} \cdot \nabla \mathbf{u}] \right) = \eta (\nabla \mathbf{u} + (\nabla \mathbf{u})^T) \quad (10)$$

where $f(tr[\boldsymbol{\tau}])$ is a function depending on the trace of the stress tensor $\boldsymbol{\tau}$, \mathbf{D} is the deformation rate tensor, λ is the relaxation time, η is the viscosity and $\overset{\vee}{\boldsymbol{\tau}}$ stands for the Oldroyd upper convective derivative.

In the literature there are two functions $f(tr[\boldsymbol{\tau}])$. The first one is the linearized function, given by,

$$f(tr[\boldsymbol{\tau}]) = 1 + \frac{\varepsilon \lambda}{\eta} tr[\boldsymbol{\tau}] \quad (11)$$

which is acceptable for low Reynolds numbers, where small molecular deformation occurs.

The second function, is exponential and is given by,

$$f(tr[\boldsymbol{\tau}]) = \exp\left(\frac{\varepsilon \lambda}{\eta} tr[\boldsymbol{\tau}]\right) \quad (12)$$

The parameter ε is related to the elongational behaviour that the model predicts.

The **Giesekus** model is given by,

$$\boldsymbol{\tau}_p + \lambda \left[\frac{\partial \boldsymbol{\tau}_p}{\partial t} + \mathbf{u} \cdot \nabla \boldsymbol{\tau}_p - \left((\nabla \mathbf{u})^\top \cdot \boldsymbol{\tau}_p + \boldsymbol{\tau}_p \cdot \nabla \mathbf{u} \right) \right] + \frac{\alpha \lambda}{\eta_p} (\boldsymbol{\tau}_p \cdot \boldsymbol{\tau}_p) = \eta_p (\nabla \mathbf{u} + (\nabla \mathbf{u})^\top) \quad (13)$$

where λ is the polymer relaxation time, α is the mobility factor, associated with anisotropic Brownian motion and anisotropic hydrodynamic drag of the polymer molecules, and η_p is the polymer viscosity coefficient.

There are other models that exist in the literature that show improvements over the models previously described. For example, we have the **FENE-P** (finitely extensible nonlinear elastic) model (Bird, Dostson and Johnson 1980) that takes into account the fact that a molecule should not be stretched infinitely. The constitutive equation is based on the evolution of the configuration tensor that can be linked to the stress tensor $\boldsymbol{\tau}_p$ by:

$$\frac{\partial \mathbf{A}_p}{\partial t} + \mathbf{u} \cdot \nabla \mathbf{A}_p - \left((\nabla \mathbf{u})^\top \cdot \mathbf{A}_p + \mathbf{A}_p \cdot \nabla \mathbf{u} \right) = -\frac{1}{\lambda} \left(f(\text{tr}[\mathbf{A}]) \mathbf{A} - a \mathbf{I} \right) \quad (14)$$

$$\boldsymbol{\tau}_p = \frac{\eta_p}{\lambda} \left(\frac{L^2}{L^2 - \text{tr}[\mathbf{A}]} \mathbf{A} - a \mathbf{I} \right) \quad (15)$$

In these equations the constant model parameter L^2 is the extensibility parameter and $a = 1/(1 - 3/L^2)$.

Another way to improve the modelling of the physical behavior of viscoelastic fluids is to use a combination of more than one constitutive equation. In this way, more relaxation times can be covered, and therefore more realistic results are obtained.

For example, the n -mode Giesekus model, would be given by,

$$\boldsymbol{\tau}_p = \sum_{i=1}^n \boldsymbol{\tau}_{pi} \quad (16)$$

with

$$\boldsymbol{\tau}_{pi} + \lambda_i \left[\frac{\partial \boldsymbol{\tau}_{pi}}{\partial t} + \mathbf{u} \cdot \nabla \boldsymbol{\tau}_{pi} - \left((\nabla \mathbf{u})^\top \cdot \boldsymbol{\tau}_{pi} + \boldsymbol{\tau}_{pi} \cdot \nabla \mathbf{u} \right) \right] + \frac{\alpha_i \lambda_i}{\eta_{pi}} (\boldsymbol{\tau}_{pi} \cdot \boldsymbol{\tau}_{pi}) = \eta_{pi} (\nabla \mathbf{u} + (\nabla \mathbf{u})^\top) \quad (17)$$

This multimode approach will be useful for the modelling of the different materials used in this work. They will allow the rheological fit to the experimental data, and will be solved numerically, allowing the prediction of the flow behaviour.

Part II Experiments, Results and Discussion

Chapter 4

4. Experimental Results and Discussion

Before presenting the obtained results for different tests and the discussion of those results, we will present a brief description of the different samples (grades) of acrylonitrile butadiene styrene (ABS) that are used along the thesis.

Samples: In this work, four different samples are studied. One of these four samples is conventional ABS in form of pellets (used for extrusion and injection moulding) and the rest of the three samples are filaments of ABS used as feedstock material in different fused deposition modelling machines. The details regarding the four different samples studied in this work can be checked in Table. 2.

Table 2 : Samples (grades) of acrylonitrile butadiene styrene (ABS) used in this study

Name	Description	Price
Sample 1	Pellets of commercial ABS (Ronfalin TRE 39) used as feedstock material for extrusion and injection molding.	2 EUR/kg
Sample 2	Commercial filament (1.75 mm diameter) of ABS (ABSNTN1) used as feedstock material for fused deposition modeling.	30 EUR/kg
Sample 3	Commercial filament (3.00 mm diameter) of ABS used as feedstock material for fused deposition modeling.	30 EUR/kg
Sample 4	Commercial filament (1.75 mm diameter) from a cartridge of ABS used as feedstock material for fused deposition modeling.	200 EUR/kg

4.1. Rheological Testing

The rheological behaviour of the four different samples is studied using two different rheometers: (1) a stress-controlled rotational rheometer (Paar Physica MCR 300) and (2) a twin bore capillary rheometer (Rosand RH10), as shown in Fig. 23. There are different choices of geometries that can be used in the rotational rheometer as explained earlier in Chapter 2, and the geometry used in these experiments was the parallel plate as it is best suited for high viscosity materials. The different tests performed using Paar Physica were (1) shear rate sweep, to measure viscosity at low shear rate (zero shear viscosity) and also the shear thinning $\eta(\dot{\gamma})$ behaviour of samples, (2) SAOS frequency sweep, to measure $G'(\omega)$, $G''(\omega)$ dynamic moduli and $\eta'(\omega)$, $\eta''(\omega)$ dynamic (complex) viscosity. Lastly, the capillary rheometer (RH10), was used for (3) shear rate sweep, to measure the shear thinning $\eta(\dot{\gamma})$ behaviour at high shear rates and to have a basic idea about the extensional behaviour of samples.

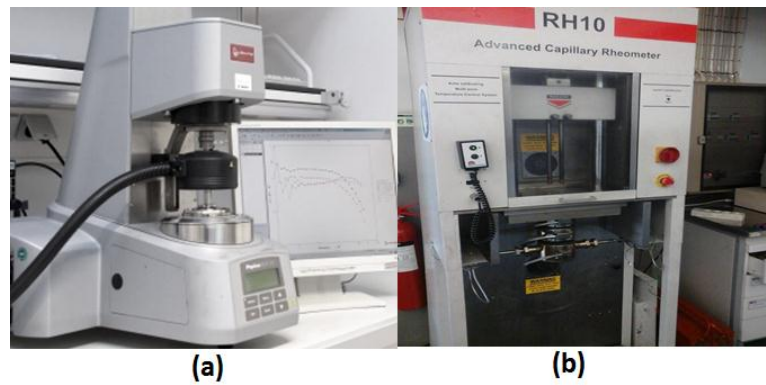


Figure 23 : Used rheometers (a) Paar physica (MCR 300), (b) Capillary rheometer Rosand (RH10)

We now present the rheological results for the four different samples. The different rheological tests, as mentioned above, were performed for three different temperatures of 220 °C, 230 °C and 240 °C, with 230 °C being chosen as the reference temperature.

The different tests performed for each one of the samples are as follows: for sample 1 and 2 all the tests mentioned above were performed at three different temperatures; for sample 3, all tests mentioned above were also performed except the high shear rate sweep, which was performed only for one temperature; lastly for sample 4 two tests were performed: low shear rate sweep and SAOS frequency sweep (for only one temperature as this sample is very expensive, and the amount of material available was small).

4.1.1. Sample 1

The shear rate sweep results for sample 1 are shown in Fig. 24, for low and high shear rates (using both of the rheometers presented before). The effect of temperature was not very prominent on viscosity, as the temperature window is not very wide, but, still viscosity decreased slightly with the increase in temperature.

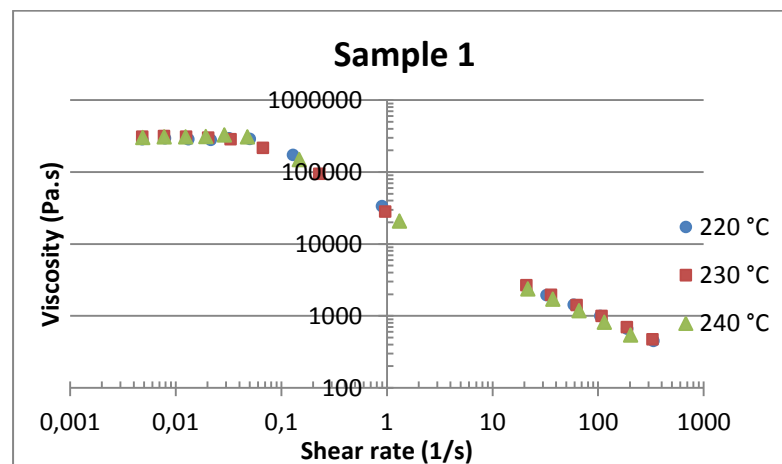


Figure 24 : Sample 1, Low & High shear rate sweep, (low shear rate sweep performed with MCR 300, and high shear rate sweep is performed using RH10)

In Fig. 24 it can also be seen that at very low shear rates the first Newtonian plateau (zero shear rate viscosity) could be captured. As the shear rate increases, viscosity decreases (shear thinning behaviour). This effect was expected, since for high shear rates the polymer chains align, thus reducing the inter-layer friction, decreasing the viscosity.

The SAOS frequency sweep was also performed at three different temperatures, and, time-temperature superposition was used to obtain master curves. These results are shown in Fig. 25, for the master curves of elastic modulus $G'(\omega)$ and viscous modulus $G''(\omega)$ at 230 °C. The SAOS frequency sweep test were performed at 5% strain which is in the linear limit of sample 1 (the linear limit is determined by performing strain sweep).

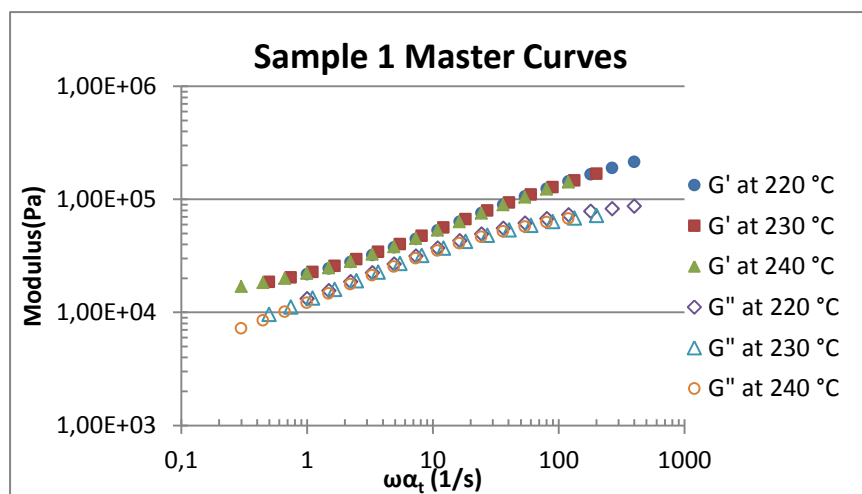


Figure 25 : Sample 1, G' and G'' master curves at 230 °C, SAOS frequency sweep

It is clear from Fig. 25, that sample 1 has high elastic behaviour, which is prominent at low as well as high frequencies. This is an indication that its structure remains intact even when the material is exposed to stress for long periods.

4.1.2. Sample 2

For sample 2, the shear rate sweep results obtained using both rheometers (for the three different temperatures) are shown in Fig. 26. The effect of temperature is not very prominent for low shear rates but is significant at high shear rates.

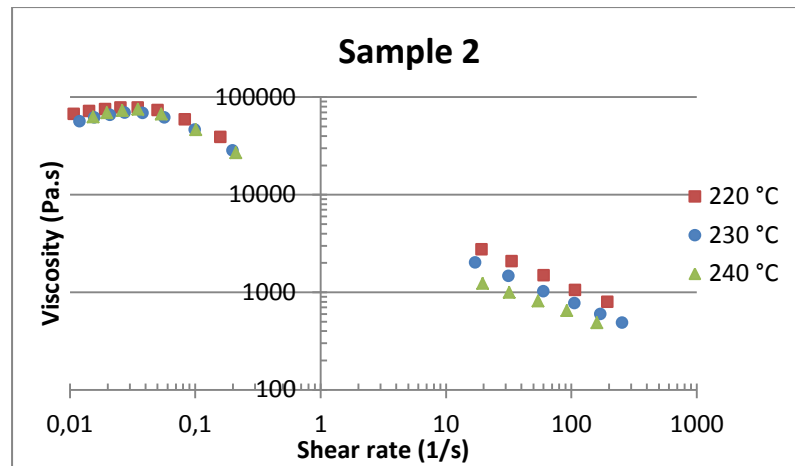


Figure 26 : Sample 2, Low & High shear rate sweep, (low shear rate sweep performed with MCR 300, and high shear rate sweep is performed using RH10)

Care should be taken when analysing these results, because, physically we were expecting bigger differences in the viscosity (for the different temperatures) at the zero shear rate plateau, and smaller differences for high shear rates. These differences may be obtained due to the intrinsic nature of the material, since for low temperature it was difficult to obtain a “melted” material, and for higher temperatures the material would degrade when exposed for long time to such temperatures (240 °C).

The master curve results (shifted to 230°C) for the elastic modulus $G'(\omega)$ and viscous modulus $G''(\omega)$ are shown in Fig. 27 (these frequency sweep tests were performed at a 4% strain which is in the linear limit of sample 2).

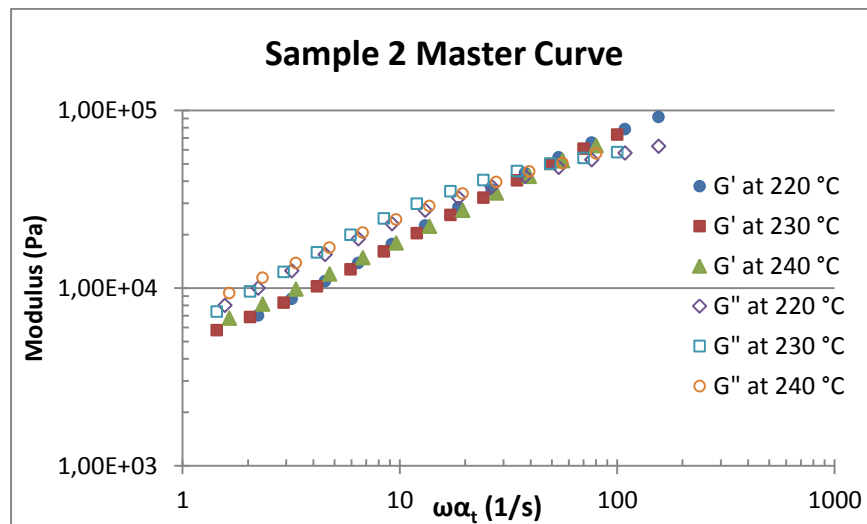


Figure 27 : Sample 2, G' and G'' master curves at 230 °C, SAOS frequency sweep

It can be seen that sample 2 has elastic response at higher frequencies and viscous response at low frequencies. There exist a relaxation time for this sample which can be found from cross over in the above graph. If the experimental time (time for which material is exposed to stress) is larger than this relaxation time, the material

will behave as a viscous liquid and if the experimental time is smaller than the relaxation time, it will behave as an elastic solid.

4.1.3. Sample 3

The previous rheological characterization was also performed for sample 3 but, due to the limited amount of material, the characterization of viscosity for high shear rates (capillary rheometer) was only possible for a temperature of 230°C.

The shear rate sweep results are shown in Fig. 28, and, it can be seen that the viscosity of sample 3 slightly decreased with the increase of temperature.

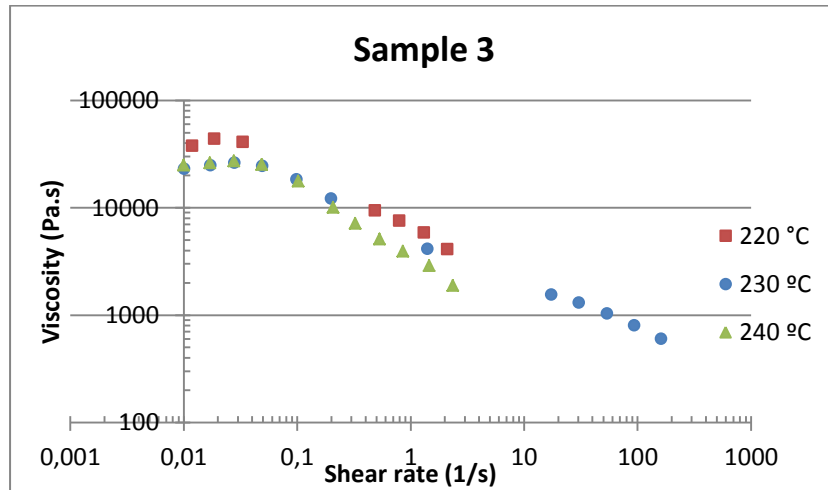


Figure 28 : Sample 3, Low & High shear rate sweep, (low shear rate sweep performed with MCR 300, and high shear rate sweep is performed using RH10)

It is clear from Fig. 28, that at very low shear rates there is a plateau in the viscosity curve, but, this plateau is not accurate. The reason for that may be the inaccuracy of the equipment at such low shear rates, and, the fact that it was difficult to “melt” the sample without degrading it.

The results of SAOS frequency sweep for sample 3 can be found in Fig. 29, for the master curves of elastic modulus $G'(\omega)$ and viscous modulus $G''(\omega)$ shifted to 230 °C. These frequency sweep tests were performed at 5% strain.

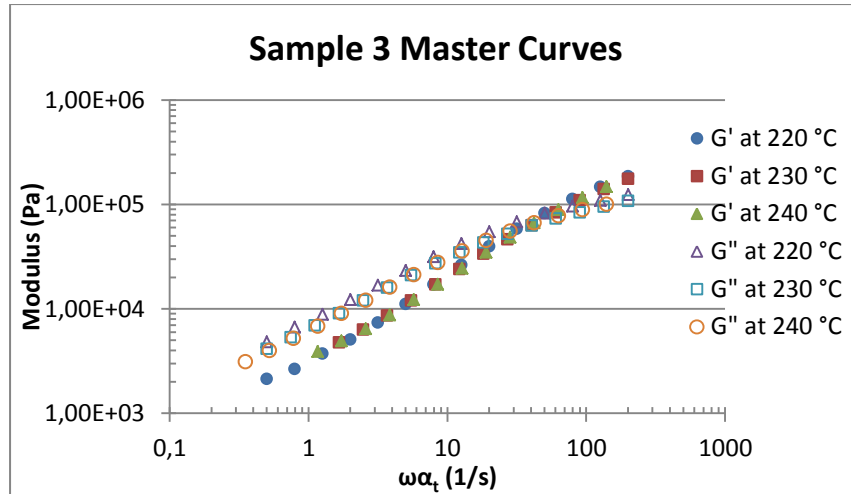


Figure 29 : Sample 3, G' and G'' master curves at 230 °C, SAOS frequency sweep

It is clear from the result of SAOS frequency sweep test that the sample 3 has similar response to the one obtained with sample 2. There is also a relaxation time for this sample which can be found from the intersection of the elastic and viscous modulus.

4.1.4. Sample 4

For sample 4, a shear rate sweep test was performed only at lower shear rates and for the reference temperature of 230 °C, as shown in Fig. 30. The reason for that was the small amount of material available and the fact that this material is very expensive.

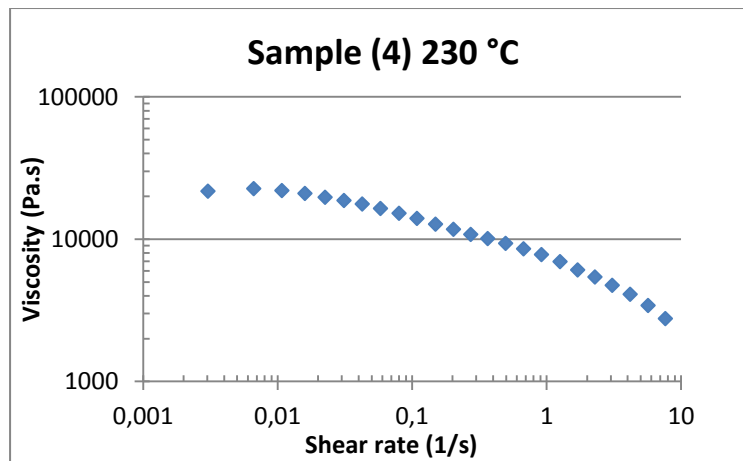


Figure 30 : Sample 4, shear rate sweep at 230 °C, obtained using MCR 300

A plateau in the viscosity curve of sample 4 can be seen at very low shear rates. The results of SAOS frequency sweep are shown in Fig. 31, (this frequency sweep test was performed at 7% strain) and it can be seen that sample 4 has a similar behaviour to that of samples 2 and 3, which, in turn, is completely different from sample 1.

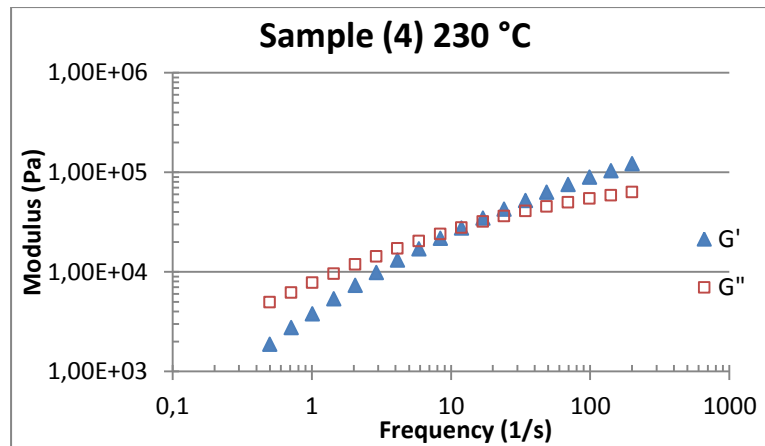


Figure 31 : Sample 4, SAOS frequency sweep, obtained using MCR 300

4.1.5. Comparison of Different Samples

The rheological results obtained for the different samples are now compared. For the rheological tests performed at the temperature of 230 °C, the sample behaved reasonably well, meaning that a “molten” state could be achieved without any degradation. Therefore, in the overall discussion, only the results obtained for 230°C will be considered.

Fig. 32 shows the different viscosities obtained for the four samples at a temperature of 230 °C.

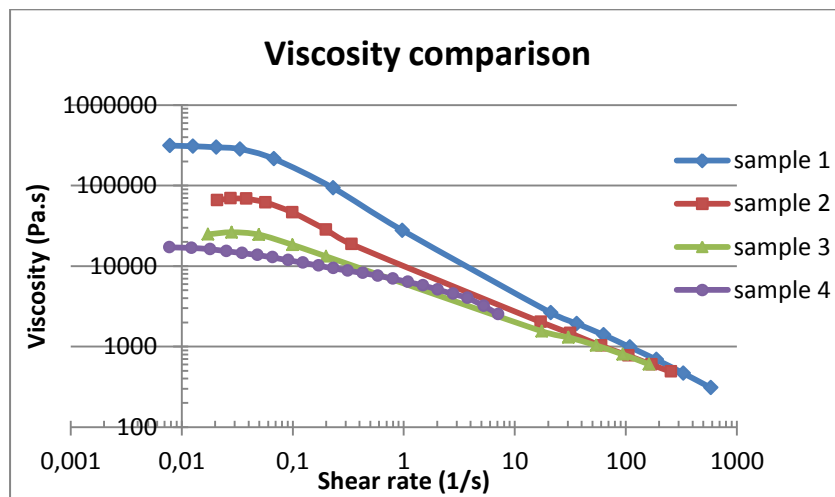


Figure 32 : Viscosity (shear rate sweep) comparison, at reference temperature (230 °C)

It is clear that the samples present a different zero shear viscosity, that is much higher for sample 1 (ABS in the form of pellets used for extrusion and injection moulding) than for other three samples (that are specifically used for fused deposition modelling process).

Normally the feedstock material used in the fused deposition modelling process has lower viscosity than the feedstock material used for injection moulding or extrusion because low viscosity materials are better candidates to have good

sintering and adhesion between extruded layers and filaments of polymer (leading to better mechanical properties of final printed products).

Another important thing associated with the viscosity of the samples is that for high viscosity it is much more difficult to extrude the material from the print head. This means that the time required for printing a specimen will increase significantly, because for high viscosity samples it requires higher residence time inside nozzle for achieving appropriate melting and decrease in viscosity.

From the above discussion, it looks like 3D printing with sample 1 will reduce quality of the process in terms of cycle time and of the mechanical properties of the printed product, but this conclusion can only be verified after printing and comparing the different materials.

The results of SAOS frequency sweep of different samples are compared in Fig. 33. These results only include elastic modulus of different samples because it is more relevant for fused deposition modelling process, as elastic modulus reflects the structure (solid like behaviour) present in the samples.

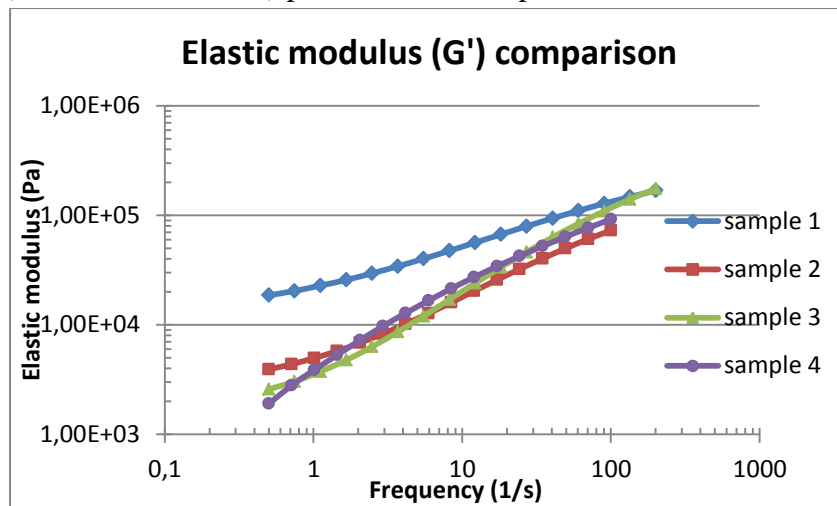


Figure 33 : Elastic modulus (G') comparison, at reference temperature (230 °C)

It can be seen that sample 1 (ABS in the form of pellets used for extrusion and injection moulding) has much higher elastic modulus than the other three samples. The elastic modulus for samples 2, 3 and 4 (ABS in the form of filaments used in fused deposition modelling process) are almost similar.

If a sample possesses high elastic modulus it means that it has stickiness and structure, and, it is difficult for such samples to flow smoothly. If the extruded sample from the print head does not flow smoothly, then it means that it will not be possible to have good sintering and adhesion, between the extruded layer and roads of samples, and, the final product will not have the desired mechanical properties. So, it is clear from the above discussion, which is based on the rheological results obtained for the different samples, that sample 1 may not produce good quality 3D printed parts.

4.2. 3D Printing of Specimens

From the previous rheological characterization results that were obtained for the four samples, we have conjectured some ideas on the quality of the printed parts. The next step is then to check the validity of the statements made before, by performing actual 3D printing.

Since the main objective of this work is to assess the feasibility of printing with materials that were not originally designed to be used in a printer, we will only compare sample 1 with sample 2 (sample 1 is the conventional ABS in the form of pellets, which is not a feedstock material for the fused deposition modelling process, and sample 2 is an ABS filament that is used as feedstock material for the fused deposition modelling process).

So, by comparing samples 1 and 2 by performing actual 3D printing, we will be able to conclude if the ABS used as feedstock material for the fused deposition modelling process have special requirements or not.

As sample 1 is available only in the form of pellets that cannot be used in the FDM process, extrusion process was used for producing its filaments (as explained earlier in Chapter 2).

4.2.1. Dimensions of the Specimens and Printing Pattern

When printing a 3D object, we first need to decide the shape and dimensions of the object. In this work, we will print 3D specimens as the one shown in Fig. 34. The reason for choosing such geometry is based on the fact that we want to perform flexural mechanical tests on the printed specimens, in order to gain some knowledge on the sintering and levels of adhesion (between the layers) obtained for the different samples.

The dimensions of the 3D printed specimens were obtained from the ASTM D790 standard. This standard also describes the test procedure used for the 3-point bending test (flexural testing).

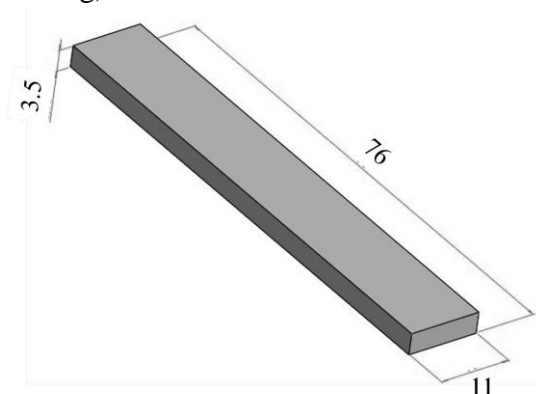


Figure 34 : 3D printed specimen, length: 76 mm, width: 11 mm, and depth: 3.5 mm

According to this ASTM standard, the length of the specimen should be 16 times its depth and the width of the specimen should not exceed one fourth of the length of the specimen (when its depth is greater than 3.2 mm). In this case, the chosen

thickness (depth) of the specimen is 3.5 mm, so the length of the specimen should be 56 mm and the width 11 mm. During the flexural testing, the specimen is placed on top of two supports, as explained in Chapter 2. The specimen should be long enough to allow for overhanging during test and to prevent the specimen from slipping over the supports; therefore, extra 20 mm were added to the length, leading to a final length of 76 mm.

After selecting the dimensions of the specimens, we selected the printing pattern, as shown in Fig. 35.

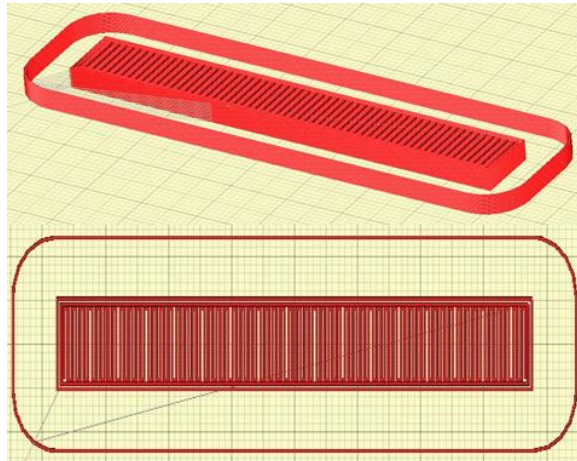


Figure 35 : Selected 3D-Printing pattern for specimens

The reason for choosing this pattern is to study the effect of sintering and adhesion between the extruded layers, since during flexural testing (when the 3 point bending test is performed) the maximum load that a particular specimen can bear will depend on the quality of the sintering and adhesion of these vertically printed roads of feedstock material. Since the thickness of the specimens is 3.5 mm, this thickness was achieved by printing 10 layers (the thickness of each layer was 0.35 mm).

4.2.2. Printing Conditions

After selecting the dimensions of the specimens and the printing pattern to be used in the 3D printing process, the next step is to choose the most suitable printing conditions. The values of different parameters used in the 3D printing process are shown in Table. 3.

Table 3 : Process parameters used in fused deposition modelling (3D printing)

3D-Printing Conditions		
Material	Sample 1	Sample 2
Extrusion temperature	230 °C	230 °C
Bed temperature	120 °C	120 °C
Speed of extrusion head	30 mm/s	30 & 50 mm/s
Solid infill	100 %	100 %
Extruded filament diameter	0.35 mm	0.35 mm
Thickness of one layer	0.35 mm	0.35 mm

As mentioned in Table 3, the extrusion temperature set for the extrusion head of the fused deposition modelling machine was 230 °C, for both samples (this is the same temperature that allowed a good rheological characterization).

Another important parameter is the bed temperature. This bed temperature should be set to a value above the glass transition temperature of the feedstock material, because, it is very important that the extruded roads of feedstock material adhere completely to the bed during printing process. On the other hand, this temperature cannot be too high or otherwise, the printed object will deform when being removed from the bed.

Glass Transition Temperature:

An important measure that can help on determining the temperature for the bed is the glass transition temperature of the material. Based on this, the glass transition for the different ABS samples was measured using a differential scanning calorimeter (DSC), as shown in Fig. 36.



Figure 36 : Differential scanning calorimeter (DSC), DSC Netzsch

The glass transition temperatures obtained for the different samples are shown in Table. 4.

Table 4 : Glass transition temperatures of ABS samples

Glass Transition Temperatures	
Sample 1	110.4 °C
Sample 2	107.3 °C

These glass transition temperatures were obtained from the curves shown in Fig. 37 and Fig. 38.

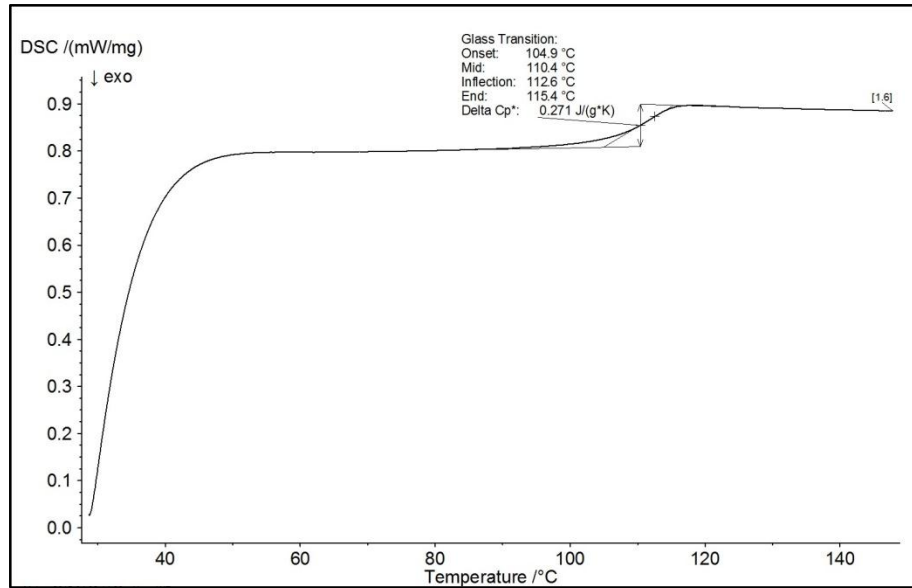


Figure 37 Sample 1: DSC results

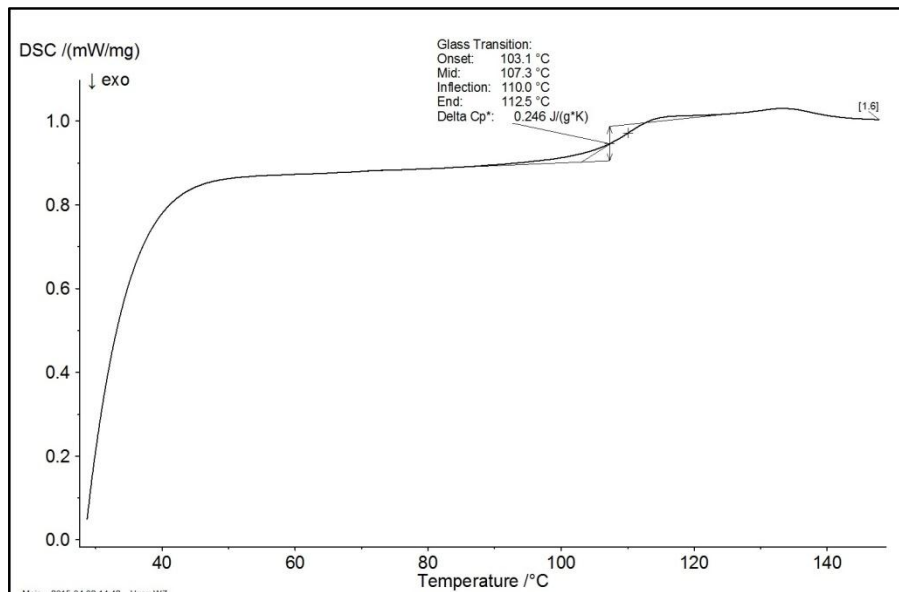


Figure 38 Sample 2: DSC results

The graphs shown above are the heating curves corresponding to the second cycle, for both samples. The second cycle heating curves were used to calculate the glass transition temperature because, when the first heating cycle starts, samples are in a solid state, and, their base is not touching the sample pan completely. In these conditions, heat transfer at the interface will not be perfect and there can be small errors in the calculations. During the second heating cycle these errors will not occur, since a perfect contact is achieved.

Based on the above results, the temperature of the bed was set to 120 °C (as shown in Table 3) during the 3D printing of the samples. This temperature is reasonably above the glass transition temperature, allowing for a good adhesion between the bed and the first printed layer.

Speed of Extrusion Head:

Another important printing variable is the speed of the extrusion head. Normally, this speed is around 50-60 mm/s for ABS feedstock materials, which is the case of sample 2. Sample 2 was printed at 50 mm/s (Table. 3). However, it was not possible to print sample 1 at this speed (50 mm/s) because it has a much higher viscosity and it does not “melt appropriately” in such a short residence time. So, sample 1 was printed using a lower speed of extrusion (30 mm/s). This is a major drawback, since the cycle time for sample 1 is almost twice as the cycle time for sample 2. Note that in order to compare the performance of the two samples, we also printed sample 2 at the lower speed of 30 mm/s.

When printing, we can set the percentage of solid infill, and, for this case we have set this parameter to 100 %, because, it facilitates the study on the sintering and adhesion behavior between the extruded filaments of the samples.

4.3. Samples Performance

In order to understand the performance of the two different samples (1 and 2) used for printing, we evaluated the sintering, bonding and adhesion by performing mechanical and optical tests. These tests consisted of the three point bending test (flexural test), optical microscopy (for the sintering and bonding between the extruded filaments) and image analysis (to quantify the amount of air or free space present in the printed specimens).

4.3.1. Flexural Testing

The three point bending test was performed using the universal testing machine, INSTRON 4505, as shown in Fig. 39. The tests were performed at room temperature, following the test procedure described in ASTM D790 standard. Four tests for each sample were performed in order to check the reproducibility of the results.



Figure 39 : Universal testing machine, INSTRON 4505

Sample 1: The result of the flexural test for sample 1 is presented in Fig. 40. This graph shows the response of the specimen when load is increased. Note that cracks are produced in the specimen with its increasing deflection.

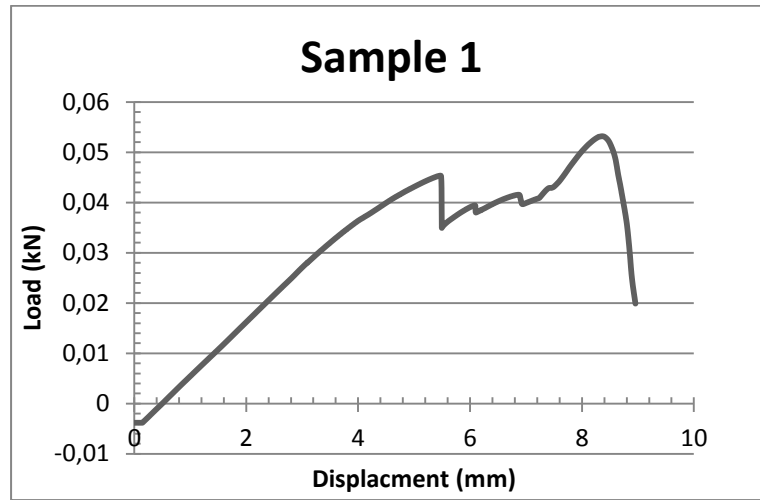


Figure 40 : Sample 1, three point bending test (flexural testing).

It is clear from Fig. 40, that the first crack is produced in the specimen when the load is around 45 N and the maximum load was obtained before failure at 53.2 N. This test was repeated four times, in order to evaluate the reproducibility of the results, and these results were consistent (Table. 5).

Table 5 : Sample 1, results of three point bending test (maximum loads at breakage)

No.	Maximum Load at Breakage (N)	Average	Standard Deviation (σ)
Specimen 1	53.2	57.4	4.02
Specimen 2	62.3		
Specimen 3	55.2		
Specimen 4	58.8		

Sample 2: Sample 2 was used to print specimens at two different speeds (30 mm/s and 50 mm/s), as explained in section 4.2.2. These results are shown in Fig. 41 and 42, and Tables 6 and 7.

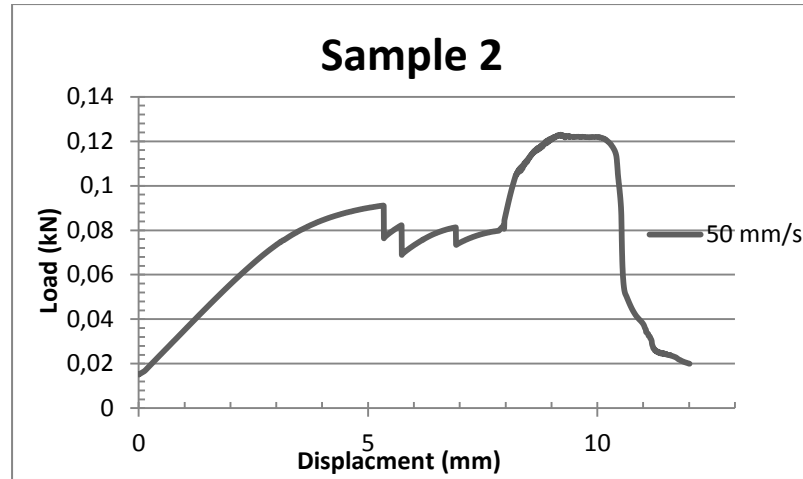


Figure 41 : Sample 2 (50 mm/s), three point bending test (flexural testing)

It can be seen, from Fig. 41 that (for a printing velocity of 50 mm/s) the first crack is produced in the specimen when the load is around 90 N, and, the total failure occurs at 122.9 N. The complete set of results is shown in Table. 6.

Table 6 : Sample 2 (50 mm/s), results of three point bending test (maximum loads at breakage)

No.	Maximum Load at Breakage (N)	Average	Standard Deviation (σ)
Specimen 1	122.8	117.1	12.5
Specimen 2	98.4		
Specimen 3	124.2		
Specimen 4	122.9		

For a printing velocity of 30 mm/s, the main findings are shown in Fig. 42 and Table 7. As explained earlier, these specimens are printed just to compare the performance of the specimens produced from sample 2 with specimens produced from sample 1, using the same 3D printing conditions.

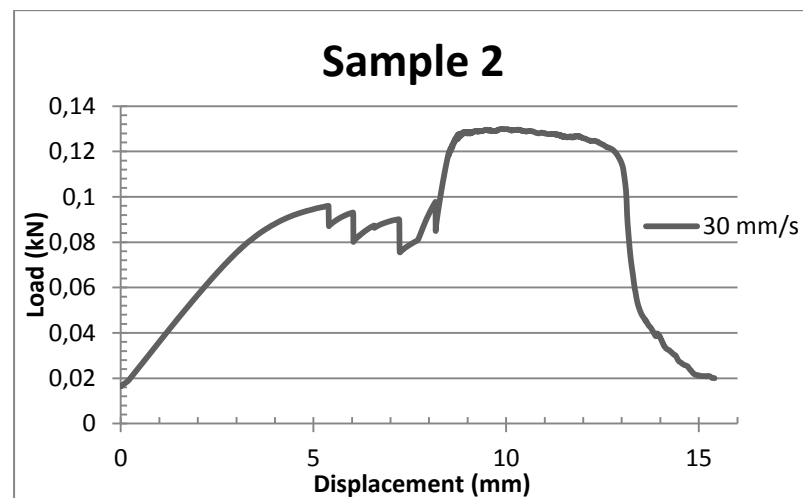


Figure 42 : Sample 2 (30mm/s), three point bending test (flexural testing)

It is clear from the above graph that the first crack is observed in the specimen when the load is around 95 N and the load at which the specimen failed completely is 130 N. The complete set of results for printing velocity (30 mm/s) is shown in Table. 7.

Table 7 : Sample 2 (30 mm/s), results of three point bending test (maximum loads at breakage)

No.	Maximum Load at Breakage (N)	Average	Standard Deviation (σ)
Specimen 1	130.6	124.5	7.08
Specimen 2	130.0		
Specimen 3	121.2		
Specimen 4	116.0		

It can be seen from the above results of flexural tests, that the specimens printed using sample 2 have better sintering and adhesion between the extruded filaments, as they require a much higher load to break. The sintering and adhesion between the extruded filaments improved when specimens were printed at a lower speed.

4.3.2. Optical Analysis

In this subsection, the surfaces of the broken 3D printed specimens (specimens which broke during flexural tests) are analysed using the stereoscopic magnifying glass Olympus and the digital camera Leica, as shown in Fig. 43.

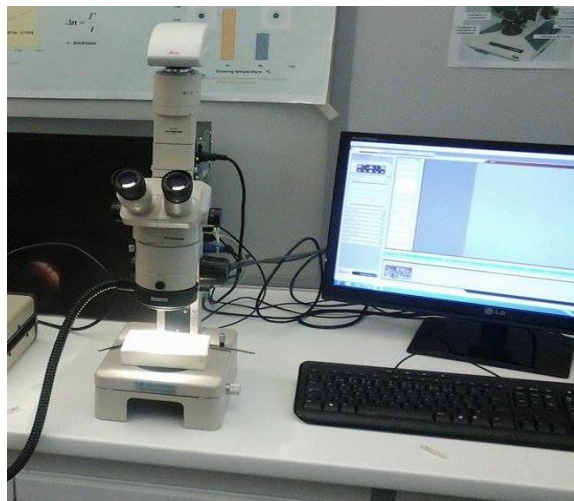


Figure 43 : Stereoscopic magnifying glass Olympus and digital camera Leica.

The analysis of the surface at the breakage section of specimens is helpful to check the sintering and adhesion achieved for extruded filaments. Image analysis was also performed in order to quantify the free space/amount of air in-between the layers for each specimen.

Sample 1: The images of the specimen's printed using sample 1 are shown in Fig 44. The images of the specimens were taken at the breakage section, which occurred during flexural testing.

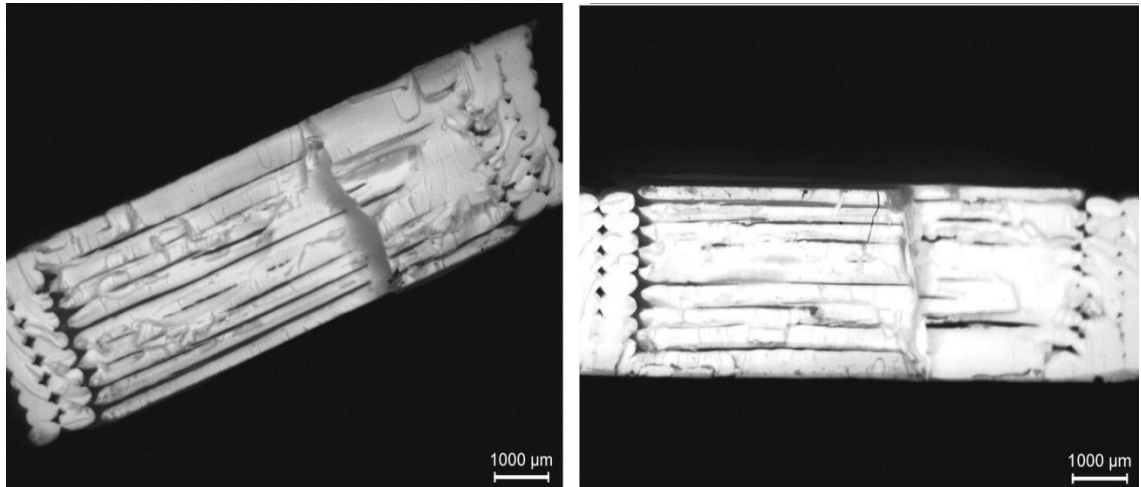


Figure 44 : Specimens printed using sample 1

It is clear from the above images that when specimens are printed with sample 1, there are many voids and free spaces in the specimens and the extruded filaments do not present a good sintering and adhesion. After doing an image analysis, the free space / amount of air found in this specimen is 5.9 % of the total area.

Sample 2: The result of the specimen's printed from sample 2 at 50 mm/s and 30 mm/s are presented in Fig. 45 and Fig. 46 respectively.

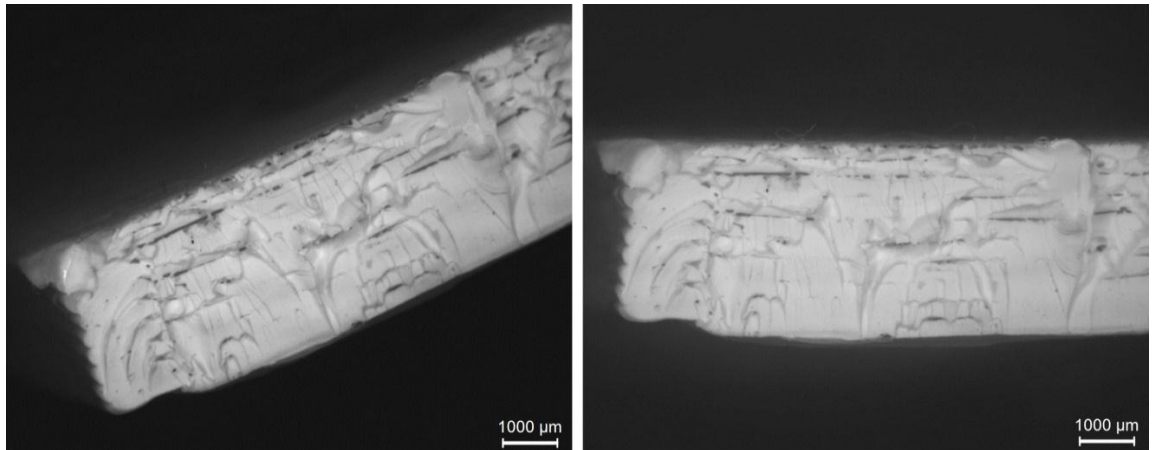


Figure 45 : Specimens printed (50 mm/s) using sample 2

In Fig. 45 it can be seen that there are relatively less voids and free spaces when compared to the results obtained for sample 1. After doing the image analysis for this specimen, the free space / amount of air found in it was 3.7 % of the total area.

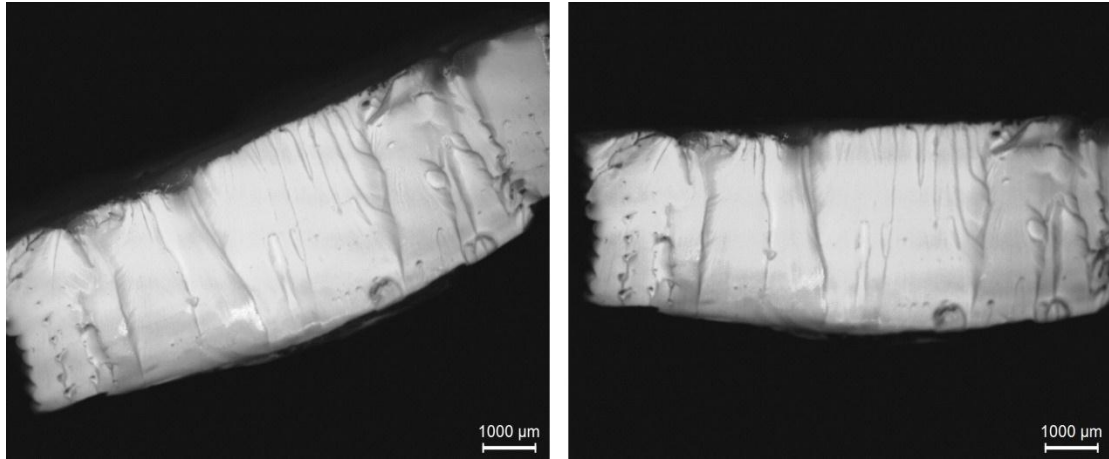


Figure 46 : Specimens printed (30 mm/s) using sample 2

It is clear from Fig. 46 that when printing (using sample 2) at a lower speed (30 mm/s), there are less voids and free space, and, the extruded filaments present very good sintering and adhesion. After doing the image analysis, the free space / amount of air found in this specimen is 0.7 % of the total area.

It can be concluded from the results of image analysis, that the specimens printed using sample 2 have much better sintering and adhesion between the extruded filaments, as they have smaller free space/ amount of air, than those printed using sample 1. The sintering and adhesion between the extruded filaments improved when specimens were printed at a low speed, as these specimens have lowest free space/ amount of air.

4.4. Global Discussion

In this subsection, a global discussion is made based on the results obtained from the rheological characterization and the 3D printing performance.

The rheological results show that sample 1 is much more viscous and elastic than samples 2, 3 and 4, and, samples 2, 3 and 4 have similar rheological behaviour. It is clear that when sample 1 is used as feedstock material in the fused deposition modelling process, a good sintering and adhesion between the extruded filaments is not achieved, thus degrading the mechanical properties of the final product. Also, the cycle time of the specimens printed using sample 1 is higher (when compared to sample 2), because it is more viscous and elastic. This means that it requires a higher residence time inside nozzle for achieving appropriate melting and decrease in viscosity, ensuring in this way, the material is properly extruded.

The flexural tests also confirmed the previous conclusions, showing that a smaller maximum load was obtained for sample 1.

For sample 2, the results were improved, especially for the specimens printed at a lower velocity of 30 mm/s. This means that at a lower speed one could achieve highest sintering and adhesion between the extruded filaments. These good results were obtained because this sample is less viscous and elastic, as compared to sample 1; secondly, sintering and adhesion for sample 2 was improved for a lower speed of

extrusion, because, at lower speeds, the residence time of the feedstock material is higher and the material becomes less viscous, allowing for a better sintering and adhesion between the extruded filaments..

Lastly, optical analysis of the printed specimens was also performed to check the quality of the sintering and adhesion. This analysis also confirmed all the statements made before, based on rheological characterization and flexural tests. Image analysis showed that the free space/ amount of air in the different specimens, was higher for sample 1 than for sample 2 (for which we obtained a good sintering and adhesion).

To conclude, it is clear that the rheological results, the 3D printing results, the flexural tests and the results from optical analysis are all in accordance.

Part III Modelling

Chapter 5

5. Numerical Modelling

In chapter 3, we have presented the equations governing the fluid flow of viscous and viscoelastic fluids. These equations will now be useful for the numerical modelling of polymer melts in the liquefier.

From the rheological characterization of the different samples, we extracted data that will allow the fitting of a rheological model to the real behaviour of the polymer melt. This data is the shear viscosity and the storage and loss modulus. From the capillary rheometer one could also obtain the extensional viscosity, assuming the validity of the Cogswell analysis (Padmanabhan and Christopher 1997), but, the results obtained were not good.

For the modelling we have used the Bird-Carreau and the FENE-P (finitely extensible nonlinear elastic) models. FENE-P model presents improvements, when compared, for example, to models that make use of Hookean springs (that allow infinite extension of the polymer molecules). In the FENE-P model, the unphysical extension of molecules to infinity is not possible. The elastic force is no more linear in the elongation and the resistance of the polymer to the stretching becomes infinite when it reaches its maximum elongation.

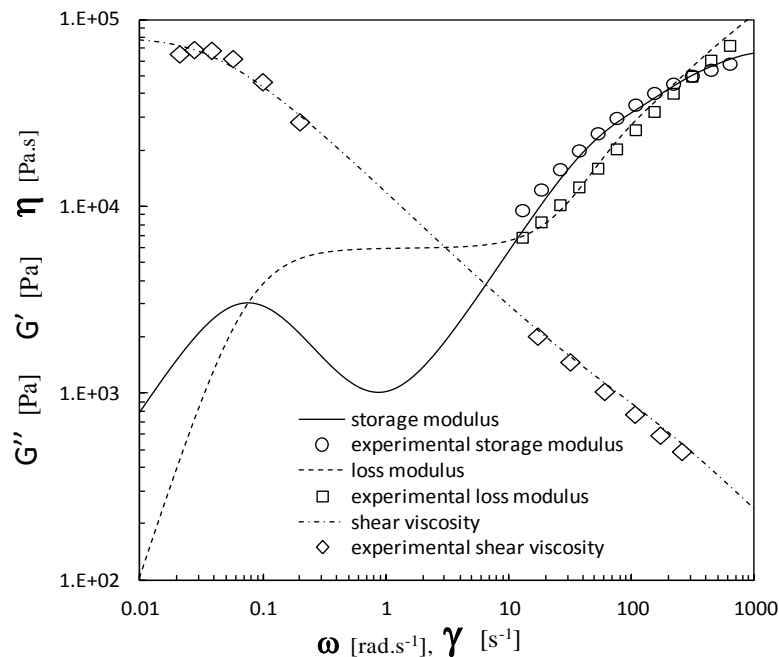


Figure 47 : Storage modulus, loss modulus and viscosity for 230 °C (experimental data and fit obtained with the 6-mode FENE-P model for sample 2)

The fit of the experimental data for sample 2 was obtained with a 6-mode FENE-P model, as shown in Fig. 47. The parameters used in the fitting are shown in Table 8.

Table 8: Parameters used in the 6-mode FENE-P model fit.

Mode	1	2	3	4	5	6
G	23916.95	5991.187	25424.19	20997.16	59360.35	47891.73
λ	0.002992	13.26889	0.014324	0.002868	6.88E-04	6.87E-04
L²	0.002754	0.484587	3.000008	0.002713	0.001047	0.001045

For sample 1 it was not possible to obtain a good fit using a viscoelastic model, therefore, first the results for sample 1 and sample 2 will be compared and discussed for the generalized Newtonian simulations (using the Bird-Carreau model for viscosity), and secondly, the difference between the viscoelastic and the viscous flow will be compared for sample 2. The fit of the shear viscosity is shown in Fig. 48 for the Bird-Carreau model.

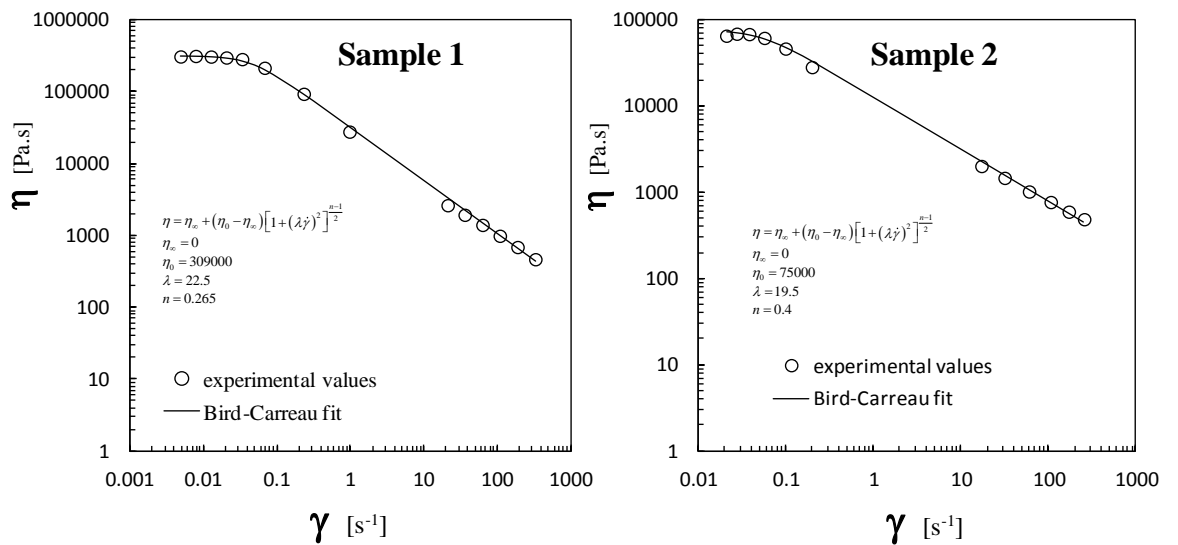


Figure 48 : Shear viscosity fit for sample 1 (left) and sample 2 (right).

Remark: It should be noted that the viscoelastic fit obtained for sample 2, was only possible assuming the loss and storage modulus are representative of the leathery region.

5.1. Geometry, Simulation and Numerical Results

The geometry used in the simulations is shown in Fig. 49. On the left we can see the nozzle screw used in the 3D printer, and on the right, a schematic of the interior geometry (where the melt flows) is shown.

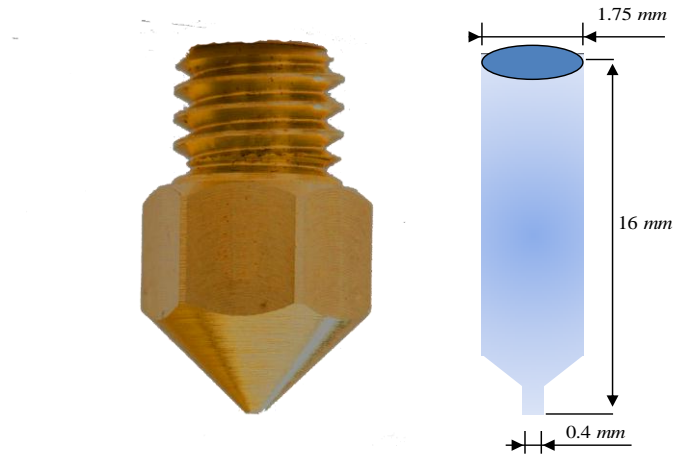


Figure 49 : 3D printer nozzle: screw (left), schematic of the geometry where the polymer melts flows (right).

5.1.1. Viscous Results

The results obtained from the numerical simulations (assuming the viscosity follows a Bird-Carreau model and assuming an initial velocity of 30 mm/s), are now shown in Fig. 50, 51, 52 and 53, for the velocity magnitude, pressure, shear and normal stresses, for samples 1 and 2.

By looking at Fig. 50, it can be observed that the higher maximum velocity magnitude is obtained for sample 2, and, that the pressure drop (Fig. 51) is smaller for the sample 2. This means that sample 2 offers lower resistance to flow, leading to the conclusion that the viscosity is smaller for this sample (as seen experimentally).

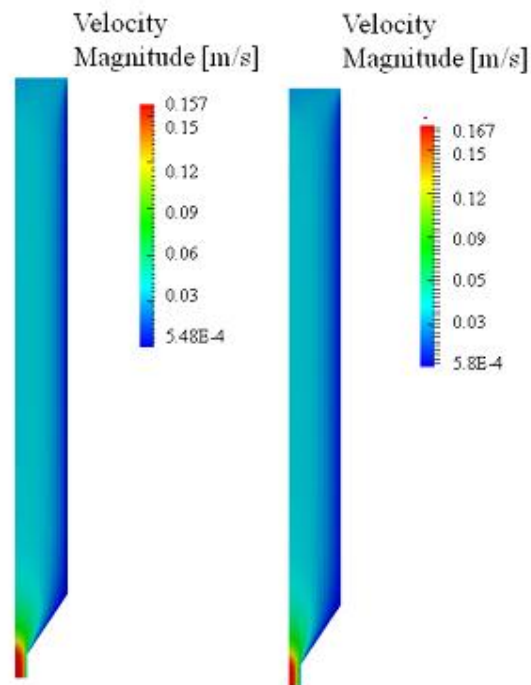


Figure 50 : Velocity magnitude for samples 1 (left) and sample 2 (right), along the channel

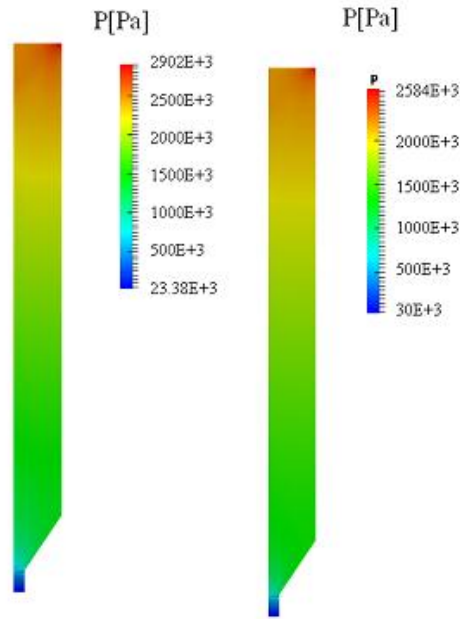


Figure 51 : Pressure for samples 1 (left) and sample 2 (right), along the channel

The shear and normal stresses along the printing nozzle, were also studied in this work, as shown in Fig. 52 and 53. The results for the different samples are similar, but, it looks like higher shear rates are obtained for sample 2 (since the viscosity is smaller, the shear rate needs to be higher, because the stress depends directly (linearly) on the viscosity).

High values of stress are obtained when the fluid enters the smaller channel, since, due to conservation of mass, the velocity increases (extension), and the restriction imposed by the no-slip boundary condition propagates to bulk of the flow by momentum, leading to shear.

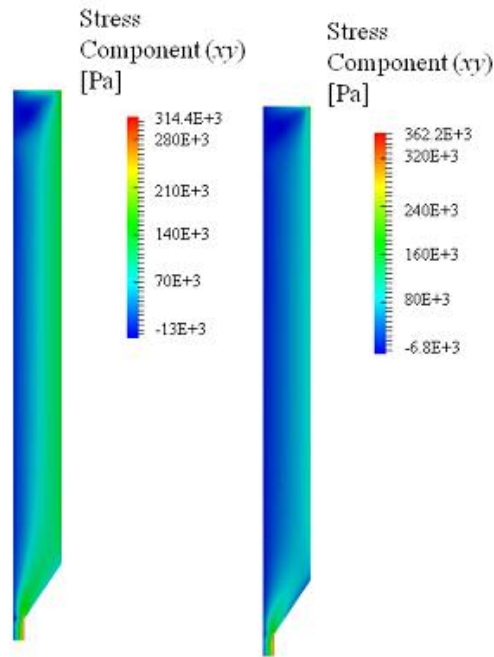


Figure 52 : Shear stress for samples 1 (left) and sample 2 (right), along the channel.

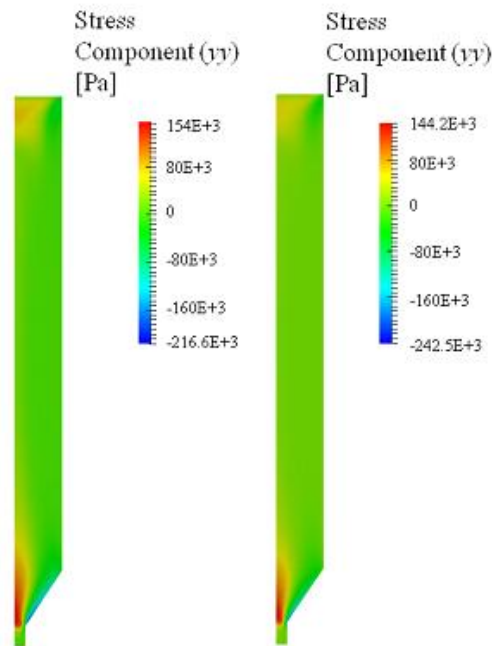


Figure 53 : Normal stress for samples 1 (left) and sample 2 (right), along the channel.

5.1.2. Viscoelastic Results

The results obtained for the viscoelastic numerical simulations of sample 2 are now presented in Fig. 54 and 55. A close analysis shows that the results follow the same trend of the results obtained with the viscous model, but with some changes in velocity, pressure drop and stresses, due to the inclusion of elasticity.

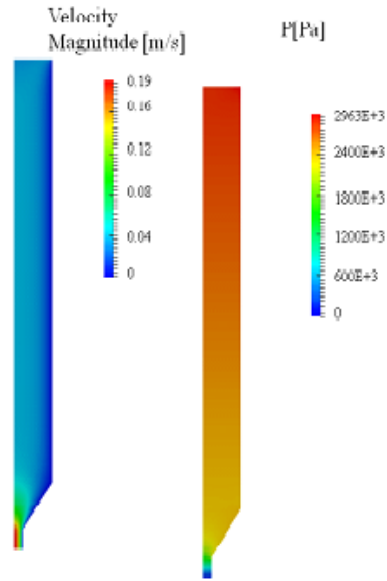


Figure 54 : Velocity magnitude (left) and pressure (right) along the channel for sample 2 (Viscoelastic simulation).

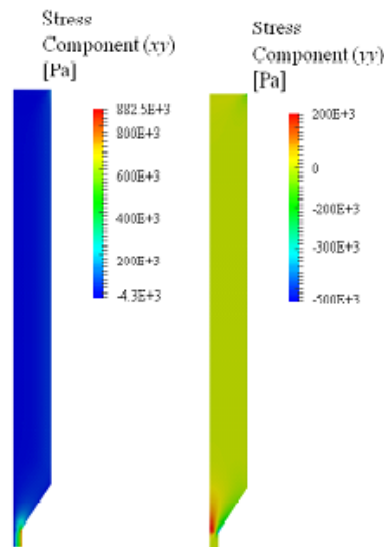


Figure 55 : Shear (left) and normal (right) stresses along the channel for sample 2 (Viscoelastic simulation).

The maximum velocity and the maximum normal and shear stresses are higher for the viscoelastic case, when compared to the viscous case (a consequence of the inclusion of elasticity).

It is worth mentioning that a detailed study of the viscoelastic case would require a good modelling of sample 1, and also, experimental data for the extensional viscosities of both samples 1 and 2. Since this is not the case, we have to rely on the results obtained for the viscous simulations, which indeed agreed with the experimental results.

Part IV Conclusions

Conclusions and Future Work

In this work the rheology of different acrylonitrile butadiene styrene samples (grades) was studied in order to evaluate their suitability for being used in the fused deposition modelling process. The rheological characterization revealed that the pelleted ABS sample (sample 1) is highly viscous and more elastic than the other three samples of ABS. Therefore, it is concluded, that this ABS, which is used for conventional polymer processing, is not as good as the other materials used as feedstock material for fused deposition modelling process.

Similarly, actual 3D printing of the different ABS samples into pre-defined geometry specimens and their mechanical and optical analysis confirmed the results obtained from the rheological characterization. It was also observed, based on the mechanical and optical analysis of the printed specimens, that good sintering and adhesion was not achieved between the extruded filaments of feedstock, for sample 1. Therefore, it can be concluded, that products printed using sample 1, does not possess good mechanical properties.

The numerical modelling of the nozzle of the fused deposition modelling machine also showed different behaviour for different samples.

Finally, based on all the above conclusions, we can say that the ABS used in fused deposition modelling process needs to have pre-defined controlled rheology, but it does not need to be “special”.

In the future, the numerical modelling of the nozzle can be improved, taking into account different convergence angles of the nozzle. During modelling it was assumed that temperature of the polymer remains constant inside nozzle, but for better results, variable temperature should be used. Finally it would be interesting to model the behaviour of the printed ABS, when the material falls on the bed of the extrusion machine.

Bibliography

- Adhesivesandglues.com. *ADHESIVES, GLUES AND SEALANTS*. 2012.
<http://www.adhesiveandglue.com/thermoplastic.html> (accessed April 12, 2015).
- Agarwala, Mukesh K, Vikram R Jamalabad, Noshir A Langrana, Ahmad Safari, Philip J Whalen, and Stephen C Danforth. "Structural quality of parts processed by fused deposition." *Rapid Prototyping Journal*, 1996: 4-19.
- Ahn, Sung Hoon, Michael Montero, Dan Odell, Shad Roundy, and Paul K Wright. "Anisotropic material properties of fused deposition modeling ABS." *Rapid Prototyping Journal*, 2002: 248-257.
- ASI adhesives & sealants. *Tailoring PSA-Dispersion Rheology for High-Speed Coating*. 27 October 2003. <http://www.adhesivesmag.com/articles/85163-tailoring-psa-dispersion-rheology-for-high-speed-coating> (accessed May 23, 2015).
- Bellehumeur, Céline, Longmei Li, Qian Sun, and Peihua Gu. "Modeling of bond formation between polymer filaments in the fused deposition modeling process." *Journal of Manufacturing Processes*, 2004: 170-178.
- Bellini, Anna, and Selçuk Güçeri. "Mechanical characterization of parts fabricated using fused deposition modeling." *Rapid Prototyping Journal*, 2003: 252-264.
- Bellini, Anna, Selcuk Guçeri, and Maurizio Bertoldi. "Liquefier dynamics in fused deposition." *Journal of Manufacturing Science and Engineering*, 2004: 237-246.
- Bhadeshia, H. K. D. H. *Differential scanning calorimetry*. University of Cambridge, Materials Science and Metallurgy, 2002.
- Bird, R.B, P.J Dostson, and N.L Johnson. "Polymer solution rheology based on a finitely extensible bead-spring chain model." *Non-Newtonian Fluid Mech*, 1980: 213-235.
- CEABLOG. *The History of 3D Printing*. 11 February 2014.
<http://www.ce.org/Blog/Articles/2014/February/The-History-of-3D-Printing.aspx> (accessed March 25, 2015).
- Chemical Book. *ABS Resins*. 2010.
http://www.chemicalbook.com/ChemicalProductProperty_EN_CB8405764.htm (accessed June 02, 2015).

- Chua, Chee Kai, Kah Fai Leong, and Chu Sing Lim. *Rapid Prototyping: Principles and Applications*. Singapore: World Scientific Publishing, 2003.
- CustomPartNet. *Fused Deposition Modeling (FDM)*. 2009.
<http://www.custompartnet.com/wu/fused-deposition-modeling> (accessed March 27, 2015).
- Donna Narsavage-Heald. *A Green Chemistry Module* . n.d.
<http://cann.scrantonfaculty.com/polymer/polymermodule.html> (accessed April 11, 2015).
- Ford, Sharon LN. "Additive Manufacturing Technology: Potential Implications for US Manufacturing Competitiveness." *Journal of International Commerce and Economics*, 2014.
- Fried, Joel R. *Polymer science and technology*. Massachusetts: Pearson Education, 2014.
- Gibson, Ian, David W Rosen, and Brent Stucker. *Additive manufacturing technologies*. New York: Springer, 2010.
- Giesekus, H. "A simple constitutive equation for polymer fluids based on the concept of deformation-dependent tensorial mobility." *Journal of Non-Newtonian Fluid Mechanics* , 1982: 69-109.
- Goderis, Bart. *Physics and Mechanical Behavior of Polymers* . Leuven: KU Leuven, Belgium, 2014.
- Gonzalez-Gutierrez , Joamin. *Thermal properties of polymers*. Ljubljana: Center for Experimental Mechanics, University of Ljubljana, Slovenia, 2015.
- Halidi, Siti Nur Amalina Mohd, and Jamaluddin Abdullah. "Moisture effects on the ABS used for fused deposition modeling rapid prototyping machine." *Humanities, Science and Engineering Research (SHUSER)*. Kuala Lumpur: IEEE, 2012. 839-843.
- Hopkinson, Neil, Richard Hague, and Philip Dickens. *Rapid manufacturing: an industrial revolution for the digital age*. John Wiley & Sons, 2006.
- Jeffrey Gotro. *Rheology of Thermosets Part 2: Rheometers*. 25 August 2014.
<http://polymerinnovationblog.com/rheology-thermosets-part-2-rheometers/#> (accessed April 04, 2015).
- Ji, Liang Bo, and Tian Rui Zhou. "Finite element simulation of temperature field in fused deposition modeling." *Advanced Materials Research*, 2010: 2585-2588.

- John R. Schrei. *Using Rheology to Improve Manufacturing*. 1 March 2002. <http://www.ceramicindustry.com/articles/83802-using-rheology-to-improve-manufacturing> (accessed April 10, 2015).
- MatWeb. *Flexural Strength Testing of Plastics*. 2014. <http://www.matweb.com/reference/flexuralstrength.aspx> (accessed April 23, 2015).
- Nikzad, MOSTAFA, SYED Hasan Masood, IGOR Sbarski, and ANDREW Groth. "A study of melt flow analysis of an ABS-Iron composite in fused deposition modelling process." *Tsinghua Science & Technology*, 2009: 29-37.
- Novakova, Marcincinova, Ludmila, and Ivan Kuric. "Basic and Advanced Materials for Fused Deposition Modeling Rapid Prototyping Technology." *Manufacturing and Industrial Engineering*, 2012.
- O'Neill, M J. "The Analysis of a Temperature-Controlled Scanning Calorimeter." *Analytical Chemistry*, 1964: 1238-1245.
- Padmanabhan, Mahesh, and W. Macosko Christopher. "Extensional viscosity from entrance pressure drop measurements." *Rheologica acta*, 1997: 144-151.
- Phan-Thien, Nhan. "A nonlinear network viscoelastic model." *Journal of Rheology*, 1978: 259-283.
- Proto3000. *Stereolithography (SLA) Services*. 2013. <http://proto3000.com/stereolithography-sla-services-rapid-prototyping.php> (accessed March 27, 2015).
- Puyvelde, Peter Van. *Additive Manufacturing of Polymers*. Leuven: KU Leuven, Belgium, 2014.
- Reddy, N V, and A Ghosh. "Fused deposition modelling using direct extrusion." *Virtual and Physical Prototyping*, 2007: 51-60.
- RedEye. *ABS*. 2015. <http://www.redeyeondemand.com/abs-thermoplastics/> (accessed June 02, 2015).
- rediff blogs. *Plastic Extrusion Machines: An Optimum way of Processing Plastics*. 01 August 2012. <http://blogs.rediff.com/trade-india/tag/processing-extrusion-machine/> (accessed April 19, 2015).
- Schowalter, William Raymond. *Mechanics of non-Newtonian fluids*. Oxford: Pergamon press, 1978.

- Shenoy, Aroon V, and D R Saini. *Thermoplastic melt rheology and processing*. New York: Marcel Dekker, 1996.
- Strong, A.Brent. *Plastics: Materials and Processing (3rd Edition)*. New Jersey: Prentice Hall, 2005.
- Sun, Q, G M Rizvi, C T Bellehumeur, and P Gu. "Effect of processing conditions on the bonding quality of FDM polymer filaments." *Rapid Prototyping Journal* , 2008: 72-80.
- Tabilo-Munizaga, Gipsy, and Gustavo V Barbosa-Canovas. "Rheology for the food industry." *Journal of Food Engineering*, 2005: 147-156.
- Thien, Nhan Phan, and I. Tanner Roger. "A new constitutive equation derived from network theory." *Journal of Non-Newtonian Fluid Mechanics*, 1977: 353-365.
- Thomas, J P, and J F Rodríguez. "Modeling the fracture strength between fused deposition extruded roads." *Proceedings of the 11th Solid Freeform Fabrication Symposium*. Texas, 2000. 16-23.
- Treehugger. *3D printing*. 2015. <http://www.treehugger.com/sustainable-fashion/3d-printing-your-party-shoes-hit-or-miss.html> (accessed March 27, 2015).
- Van der Vegt, A K. *From polymers to plastics*. Delft: VSSD, 2006.
- Venkataraman, N, et al. "Feedstock material property-process relationships in fused deposition of ceramics (FDC)." *Rapid Prototyping Journal*, 2000: 244-253.
- W.J. Briels. *The tube model*. October 1998.
<http://cbp.tnw.utwente.nl/PolymeerDictaat/node62.html> (accessed April 11, 2015).
- Wang, Tian Ming, Jun Tong Xi, and Ye Jin. "A model research for prototype warp deformation in the FDM process." *The International Journal of Advanced Manufacturing Technology*, 2007: 1087-1096.
- Yardimci, Muhammad Atif, Takeshi Hattori, Selcuk I Guceri, and Stephen C Danforth. "Thermal analysis of fused deposition." *Proceedings of Solid Freeform Fabrication Conference*. Texas, 1997. 689-698.